First-principles modeling of dye-sensitized solar cells: From the optical properties of standalone dyes to the charge separation at dye/TiO2 interfaces

Valentin Diez-Cabanes, Simona Fantacci, Mariachiara Pastore

Chapter 9

First principles modeling of dye-sensitized solar cells: from the optical properties of standalone dyes to the charge separation at dye/TiO_2 interfaces

Valentin Diez-Cabanes,[a,b] Simona Fantacci[c] and Mariachiara Pastore[a]

[a] Laboratoire de Physique et Chimie Théoriques (LPCT), Université de Lorraine & CNRS, UMR 7019, 54000, Nancy, France

[b] Laboratoire Lorrain de Chimie Moléculaire (L2CM), Université de Lorraine & CNRS, UMR 7053, 54000, Nancy, France

[c] Computational Laboratory for Hybrid/Organic Photovoltaics (CLHYO), Istituto CNR di Scienze e Tecnologie Chimiche "Giulio Natta" (CNR-SCITEC), Via Elce di Sotto 8, 06123 Perugia, Italy

[NON PRINT ITEMS]

Abstract: In this chapter we present an exhaustive overview of the recent theoretical models and computational strategies developed to afford a realistic description of the different device components integrating dye sensitized solar cells (DSSCs), and the complex physical-chemical phenomena taking place at their interfaces. Here we discuss first-principles modelling of transition metal complex (TMC) dye sensitizers and their interaction with the TiO_2 semiconductor models, with the aim of showing how theory can effectively lead toward the successful exploitation of the rich photophysics of these materials in the DSSCs field. Overall, we show how these calculations, combined with the

appropriate experimental measurements and data-driven analysis, can be opportunely used to set up useful design rules for the optimization of the properties of the different device components, as for instance, extension into the Vis-nIR (visible-near infrared) absorption window and lifetimes of the dye sensitizers, or optimization of the charge separation at the dye/semiconductor interface.

Key Words: Dye sensitized Solar Cells (DSSCs); transition metal complex dyes; hybrid inorganic/organo-metallic interfaces; DFT/TD-DFT; relativistic effects; excited state decays.

Contents

1. **Introduction**

The application of the fundamental principles and computational methodologies described in the previous chapters is at the heart of the understanding of the photophysical processes driving the operation of many light-driven technologies. One prototypical example of these technologies is based on the exploitation of solar light to produce clean energy. As a matter of fact, the sun is supplying an unlimited amount of energy in form of irradiation to the Earth surface, which can be converted into electricity by means of photovoltaics (PV) devices.[1] In this viewpoint, PV technologies appear as one of the most attractive strategies to shift towards more sustainable sources of energy, which will potentially enable, or at least contribute to, the reduction of the pollution generated by the human activities, and the supply of energy for a continuously growing population.[2] Nowadays, most of commercial solar cell technologies are built by the integration of amorphous Si (a-Si) based materials as photoactive semiconductors,[3] which indeed present several drawbacks such as high economic and environmental cost of production, large mechanical rigidity or low device performances for low intensity light sources. Alternatively, during the last decades intensive research efforts have been devoted to the development of the so-called "*third generation solar cells*", characterized by lower costs, high flexibility, and integration of earth abundant materials.[4] Nonetheless, their commercial exploitation has been hampered by their relatively low device efficiencies in comparison with the ones achieved by crystalline (but high cost manufacturing) materials (GaAs, InP).[5] Currently, the most promising technologies of this generation are the dye sensitized solar cells

(DSSCs), the organic photovoltaics (OPVs) and the perovskite solar cells (PSCs). In this chapter we will focus on the first type of solar cells, whereas the other two technologies will be discussed in detail in the subsequent two chapters of this book. Notably, DSSCs present the advantages of requiring simple preparation methods, having an excellent flexibility, good stability and being exploitable for indoor applications, since they can work under diffuse-light conditions.[6,7]

Although evidence of charge injection from an organic dye into a semiconductor in an electrochemical cell was reported at the late 1960s,[8] only in 1991 O'Regan and Grätzel achieved the first practical use of dye sensitizers grafted onto mesoporous semiconductor films to generate an electric current,[9] paving the way to massive research efforts and industrial interest in the DSSC technology.[10] The main components and the basic device operation for a typical n-type DSSC (Grätzel's solar cell) are represented in Figure 1. The functioning mechanism involves the following steps: (1) the dye sensitizer absorbs the solar light and is promoted to a charge-separated electronically excited state (D^*); (2) the photogenerated electron is injected into the conduction band (CB) of the semiconductor, where the dye sensitizers are grafted; (3) the dye recovers its neutral state (D) by transferring the photogenerated hole to the electrolyte redox mediator, (4) which is then regenerated by the reduction prompted by the metallic counter-electron acting as catalyst, thus closing the circuit which is sealed by means of a transparent conductive oxide (TCO) layer, and finally generating the electric current.[11,12]

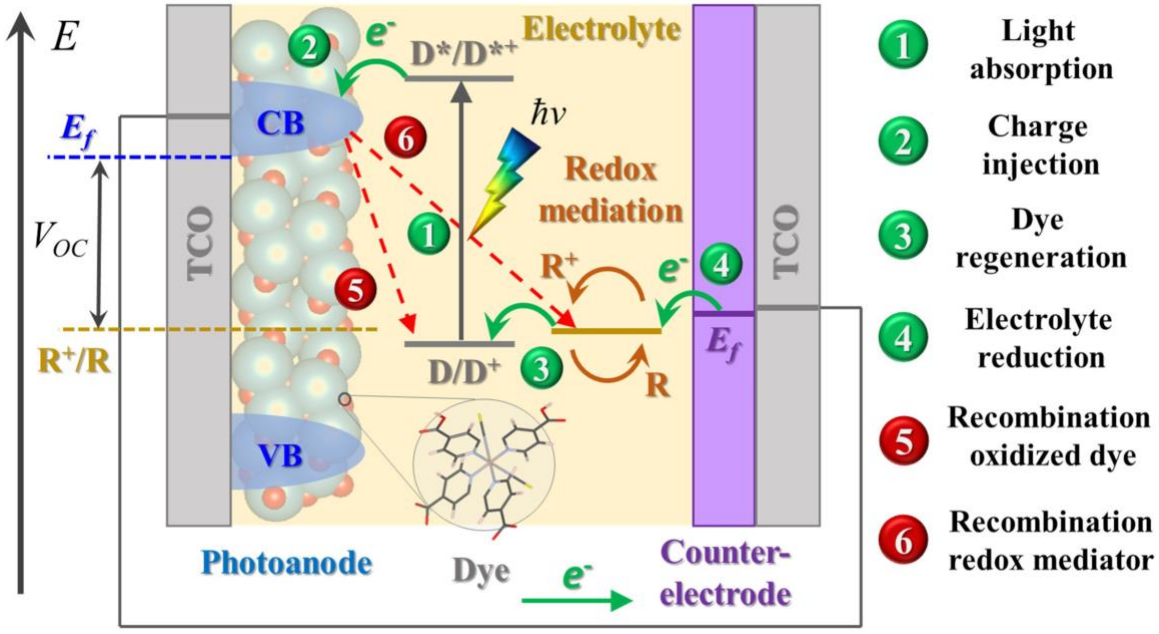

Figure 1. Scheme of the device operation of a prototypical n-type DSSC presenting the diagram for the energetic levels of the cell components. Continuous green/orange arrows are used to indicate the desired flow of electrons and redox shuttle reactions, whereas dashed red lines depict the undesired recombination processes. The numbering with all the steps involved in the process of current generation appears on the right side of the image.

As it is schematized in the energy diagram of Figure 1, the difference between the quasi-Fermi level (E_f) of the photoanode under illumination and the redox mediator potential (R^+/R) will determine the potential generated by the cell (the so-called open circuit voltage V_{OC}). Then the corresponding overall efficiency is calculated as follows:

$$\eta = \frac{V_{OC} * FF * J_{SC}}{P_I} \quad (1)$$

Where *FF* (Fill Factor) is a dimensionless parameter which reflects the internal and external cell resistances, J_{sc} is the photocurrent density at short circuit, and P_I is the intensity of the incident light. In this context, J_{sc} is estimated as the integral over the solar spectrum of the monochromatic incident photon to current conversion efficiency (IPCE) at short circuit, which can be quantified by following this equation:

$$\text{IPCE} = \text{LHE} * \phi_{inj} * \phi_{coll} \quad (2)$$

Table 1. Solar cell device characteristics for the four most performant DSSCs devices reported in the literature for each dye sensitizer family mentioned in the text. For all devices reported here, mesoporous TiO_2 was used as photoelectrode.

Family	Dye	anchoring	Redox	CE	η	Year	Ref
D-π-A organic	ALEKA-1/LEG1	silyl/COOH	$[Co(phen)_3]^{3+/2+}$	GNP/Au	14.3	2015	[13]
	XY1b/Y123	CN-COOH	$[Cu(tmby)_2]^{2+/+}$	PEDOT	13.1	2018	[14]
	ZL003	COOH	$[Co(bpy)_3]^{3+/2+}$	Pt	13.6	2019	[15]
	MS5/XY1b	CN-COOH	$[Cu(tmby)_2]^{2+/+}$	PEDOT	13.5	2021	[16]
Zn(II) Porphyrin	GY50	COOH	$[Co(bpy)_3]^{3+/2+}$	Pt	12.8	2014	[17]
	SM315	COOH	$[Co(bpy)_3]^{3+/2+}$	GNP	13.0	2014	[18]
	SM342/Y123	COOH	$[Co(bpy)_3]^{3+/2+}$	GNP	12.7	2017	[19]
	SGT-021/SGT-149	COOH	$[Co(bpy)_3]^{3+/2+}$	Pt	14.2	2020	[20]
Ru(II) complex	CYC-B11	COOH	Z960	Pt	11.5	2009	[21]
	C106	COOH	EL02	Pt	12.1	2010	[22]
	C101	COOH	I^-/I_3^-	Pt	11.7	2011	[23]
	N719	COOH	I^-/I_3^-	PtCoFe	12.3	2017	[24]
Fe(II) complex	C1	COOH	I^-/I_3^-	PEDOT	0.9	2020	[25]
	ARM13	COOH	el3(MgI_2/TBAI)	PEDOT	1.4	2021	[26]
	ARM130	COOH	el3(MgI_2/TBAI)	Pt	1.8	2021	[27]
	FeCD	COOH	$[Co(bpy)_3]^{3+/2+}$	Pt	1.3	2021	[28]

GNP=graphene nanoplatelet; FeCD=$[Fe(cpbmi)(dtapbmi)]^{2+}$; CE=counter electrode; phen=phenanthroline; tmbpy= 4,4',6,6'-tetramethyl-2,2'-bipyridine; TBAI=tetrabutylammonium iodide salt.

Being LHE the light harvesting efficiency of the photoelectrode; ϕ_{inj} the quantum yield of electron injection; and ϕ_{coll} the electron collection efficiency at the TCO. Overall, we can thus conclude that cell efficiency will be governed by the competition between the desired operation processes, involving generation, transport, and collection of charges (steps 1-4 indicated by green arrows in Figure 1), and the charge recombination losses (steps 5-6 marked with red- dashed arrows). The first reported efficiency for DSSCs in 1991 amounted to 7.1%,[9] and after three decades of active research in the field, the efficiency for these technologies has been pushed until reaching 14.3% [13] (see Table 1) under standard solar light irradiation,[29] and above 34% when employing artificial light sources.[16,30] Such an improvement in the device efficiencies has been realized by a careful optimization of the working conditions and the device components integrating the cell.[31]

The most common semiconductor materials employed as photoanodes in DSSCs are mesoporous films of TiO_2 nanocrystals due to their enhanced surface contact area where the dyes are grafted, thus significantly boosting the light harvesting. The most recent advances achieved in the TiO_2 film optimization concern the control of the characteristics (porosity, chemical composition) of the material in order to tune the interface with the electrolyte and the conductive glass, or to modify its intrinsic properties via doping or light scattering.[32,33] Other type of nanomaterial morphologies employed in DSSCs photoanodes include nanosheets, nanowires, nanorods, nanofibers.[34] Alternatively, other materials such as ZnO[35,36] and SnO_2[37,38] nanostructures, have been used as photoanodes in DSSCs as well but, unfortunately, their lower chemical stability under

illumination and their deeper CB edge energies, respectively, have somehow lowered their device efficiencies (no more than 7.5%[39] and 6.4%[40] for ZnO and SnO_2 photoanodes, respectively). It is noteworthy to mention that, in the classical Grätzel's solar cell, the working electrode consists of a n-type semiconductor where the photogenerated electrons are injected. However, the flow of electrons in the cell can be reversed by using the dye sensitizer to transfer holes into the valence band (VB) of a p-type semiconductor, which is acting as photocathode (normally NiO),[41] forming the so-called p-type DSSC. Despite this idea was firstly introduced in 1999 by Lindquist et al., the device efficiencies achieved by p-type devices were negligible.[42] A promising avenue consists in combining a photoanode and a photocathode in a tandem device which enables to collect efficiently a larger amount of solar light, thus pushing the theoretical maximum performance which can be achieved by a single-junction device up to a Shockley–Queisser limit of 43%.[43] Nonetheless, the rapid recombination taking place at the photocathode resulted in rather limited overall efficiencies, being 4.1% the largest one reported to date for tandem DSSCs devices.[44]

Regarding the materials employed for the transport of the photogenerated holes and electrons, the most common family is the one represented by liquid electrolytes made of organic, inorganic or ionic solvent coupled with a redox mediator.[45,46] The most widely employed redox couple is I^-/I_3^-, due to its suitable potentials for many dyes, good solubility and high conductivity. In spite of this, nowadays the most efficient DSSCs are systemically fabricated by employing transition metal complexes (TMC), such as Cu(II/I) or Co(III/II) based electrolyte, in view of their improved stability and their excellent electrochemical behavior.[47,48] Nevertheless, for the commercial exploitation of DSSC technologies it

would be highly desirable to avoid the use of liquid components, by replacing traditional electrolytes with quasi-solid and solid hole transport materials (HTM) such as small organic molecules, polymers, inorganic or metal complex materials, forming the so-called solid-state DSSCs (ssDSSCs).[49,50]

On the other hand, Pt based materials have dominated the role of counter electrodes in DSSCs technologies during several decades due to their excellent conductivity and catalytic activity.[51,52] However, during the last years some increasing efforts have been devoted to use catalysts displaying a better energetic alignment with the typical TMCs used as redox couples, and based on Earth abundant materials.[53,54] Among them, carbon materials such as graphene or polymers (i.e. PEDOT:PSS) alone or combined in the form of hybrid junctions have shown the best device performances (see Table 1).

Finally, as one can expect, the dye sensitizer is one of the principal ingredients of a DSSC and, its chemical versatility offers a huge space to boost the device efficiency by modulating the optical and redox properties.[55] An highly-efficient dye should possess, indeed, a wide and intense optical absorption in the Vis and nIR regions associated to a long-lived charge transfer (CT) excited state, possibly electronically coupled to the oxide CB states, and ground and excited state oxidation potentials which properly match the redox potential of the mediator and the semiconductor CB, respectively, as it is shown in Figure 1. We can mention here three main families of dye sensitizers due to their historical relevance and their higher power conversion efficiencies when employed in DSSCs: the push-pull organic sensitizers, the porphyrin-based, and the TMC dyes.[56,57]

Push-pull organic dyes possess an electron donating groups (D) connected to an electron withdrawing moiety (A) via π-conjugated bridges (also known as D-π-A architecture).[58] In addition to their high tunability and good absorption in the red portion of the solar spectrum, organic dyes also present the advantage of being metal-free materials, allowing for simple synthesis procedures, low production costs and reduced environmental impact.[20,59,60] Thanks to their long excited state lifetimes and their strong absorption in the Vis region, [61,62] Zn(II) porphyrins combined with D-A groups have emerged as highly performant sensitizers, with record efficiencies of about 13%.[18] Furthermore, their main disadvantage, represented by their tendency to aggregate at the liquid/solid semiconductor interface, can be effectively mitigated, as shown by the record reported efficiencies of 14.2%,[20] by using them in combination with other types of dye (i.e. organic D-π-A ones) in co-sensitized devices. Undoubtedly, TMCs, with Ru(II) polypyridyl complexes holding the place of honor, are historically the most studied and employed sensitizers in DSSCs applications. As a matter of fact, these dyes were the first ones to be integrated in DSSCs devices in the pioneer work of Grätzel and O'Regan,[9] and the ones displaying the largest efficiencies till the last decade (see Table 1). TMCs possess many desirable properties such as a favorable photoelectrochemical behavior, high stability of their oxidized states, and a wide absorption range from the Vis to the nIR regime. However, the main reasons behind the success of Ru(II)-based sensitizers are the long lifetime and the excellent directionality of their metal-ligand charge transfer (MLCT) states, as we will explain in more detail in the last three sections of this chapter.[63–65] Unfortunately, these dyes present important drawbacks, which have significantly limited

their commercial application, such as low extinction coefficients and, more importantly, the scarcity and potential toxicity of ruthenium.[66] Thus, during the last years the field of TMC sensitizers is moving towards the development and the use of compounds owing earth-abundant and ecologically friendly first row d-block metal centers,[67] such as Cu[68,69] and Fe[70]. Notably, $[Cu(bpy)_2]^+$ exhibit similar photophysics as the $[Ru(bpy)_3]^{2+}$ complexes[71] (*vide infra*) but their lower absorption coefficients in the Vis region and their facile ligand redistribution have hampered their use as sensitizers.[66] Despite these issues can be partially solved by means of ligand functionalization, the efficiencies achieved by Cu(I) complex sensitizers have not exceeded 4.7%.[72]

In case of Fe, even if displaying the same d^6 electronic configuration as Ru, its photophysics is completely different,[70] as we will further develop below, thus resulting in relatively low device efficiencies (Table 1). Nonetheless, due to their high technological relevance (iron is the fourth most common element in the Earth's crust), there is a growing interest in exploiting its peculiar photophysics.[73] The first attempt to employ Fe complex dyes as sensitizers was reported in the late 1990s by Ferrere and coworkers[74,75] who synthetized Fe(II) polypyridine complexes displaying similar chemical structure as the prototypical Ru(II) complexes used in DSSCs devices (N3 and N719 in Figure 2 left). However, as we will better explain in section 4, the populated metal to ligand CT (MLCT) excited states of these dyes undergo an ultrafast deactivation into metal centered (MC) states,[76] thus impeding the electron injection into the electrode and their practical application in photovoltaics. Notably, the biggest breakthrough for the development of Fe sensitizers came only in 2013 with the use of N-heterocyclic carbene (NHC) ligands to replace the traditional polypyridyl metal binding groups (see Figure 2 right).[79] The

strong σ-donor character of these ligands is able to effectively destabilize the low-lying MC states,[77,78] thus impeding the ultrafast MLCT deactivation and allowing to reach excited states lifetimes in the ps scale. For example, MCLT lifetimes of 16-18 ps were reported for the homoleptic Fe(II)-NHC complex (**C1**) [79–81] endowed with the carboxylic functionalities required to be grafted to the TiO_2 electrode. A further improvement of the excited state lifetimes can be reached via modification of the NHC ligands,[82,83] by increasing, for instance, the ligand aromaticity, [81] or by employing diazene central cores.[84] Remarkably, nowadays ligand engineering has allowed Fe-carbene complexes to reach MLCT state lifetimes in the ns scale.[85]

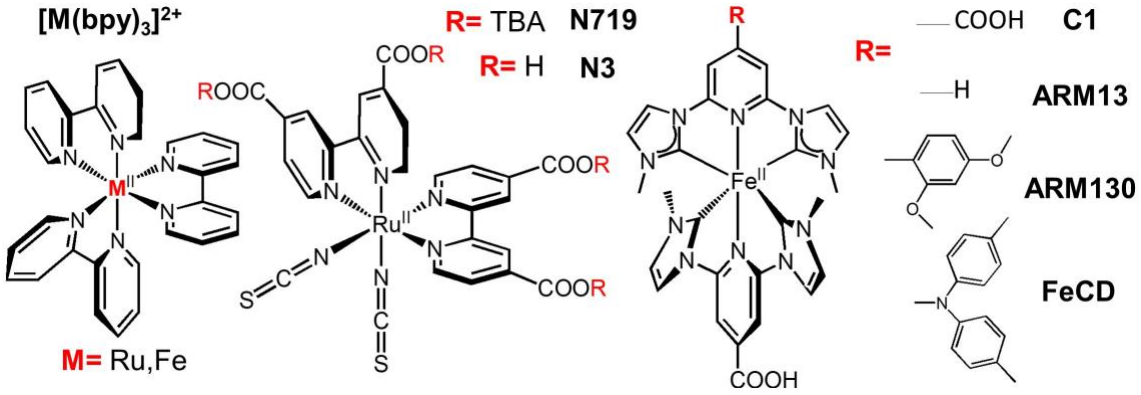

Figure 2. Chemical structures of the most performant Ru(II) (left) and Fe(II) (right) complex dye sensitizers according to Table 1.

Despite the overall improved lifetimes, efficient utilization of Fe-dyes in DSSCs is still limited, with the highest device efficiencies amounting to 1.83% (ARM130 in Table 1),[27] being still about 6-7 times lower with respect to those of Ru(II)-based solar cells. However, this field is still at its infancy (note that in the last two years the device efficiencies reported

for Fe-DSSCs have been boosted by one order of magnitude) and there is still plenty of room to improve the interfacial charge separation, for instance, via the incorporation of electron accepting moieties close to the anchoring groups, or further tuning the redox shuttles or the electrodes.

As attested by the huge number of theoretical and computational studies published in the last decades, frequently carried out in close collaboration with experiments, first principles calculations have been proved to be extremely useful to shed light on the optoelectronic properties of both the individual dyes and their interface with the electrodes and the electrolyte environment,[86–91] effectively contributing to boost the device efficiencies.[92,93] The rationalization of the main physical processes underlying the device operation via theoretical modeling has driven, indeed, the development of DSSCs technologies.[6] In this viewpoint, here we will discuss the application of the state-of-art first principle calculations to the field of DSSCs, focusing our attention on the TMC dyes. We refer the reader to some recent reviews to get a deeper knowledge of the recent advances of DSSCs technologies,[6,7,10] and of the modeling of other dye families.[90,91,94]

We will start by a short overview of the methodologies and models which have been employed in the DSSCs field in order to simulate the properties of the dye sensitizers and their interface with the TiO_2 semiconductor. Afterwards, we will illustrate how these methods can be suitably employed for describing the optoelectronic properties of TMC sensitizers. Firstly, we will discuss the last advances in modelling Ru(II) dye sensitizers,

focusing on the development of panchromatic dyes via the enhancement of their singlet-triplet states coupling. Afterwards, we will show how modelling of the dye's photophysics can be used to rationalize and optimize the MLCT state lifetimes in Fe(II) complexes. To conclude, we will illustrate how appropriate modeling of the electrode/dye/electrolyte interfaces can be used to get a better understanding of the different injection/recombination processes responsible of the photocurrent generation, and how these calculations can guide in the design of complexes leading to improved interfacial charge separation characteristics.

2. Computational Modeling of DSSCs: methods, limitations, and practical strategies

2.1 Generalities

As it is exemplified in Figure 1, DSSCs are rather complex systems involving components and processes of different nature and this makes their theoretical investigation an extremely challenging task. From a computational point of view, it is compulsory to develop realistic models and accurate methodologies to reliably describe the main properties of the cell components (dye sensitizers, semiconductor, and electrolyte) and the interactions between them. The fundamental information that one can get from atomistic simulations is: i) the dye's ground and excited state equilibrium structures, ground state oxidation potential (GSOP), optical absorption spectra and excited state oxidation potential (ESOP); ii) the semiconductor band gap and conduction and valence band density of states; and iii) the electrolyte/hole conductor redox properties.

The models employed to reproduce the TiO_2, or more in general, semiconductor surfaces can be periodic 2D slabs or finite clusters (nanoparticles) systems.[95] The choice will depend on the targeted properties and on the appropriateness of the finite models in reliably reproducing the electronic structure of the solid material. For instance, TiO_2 nanoparticles[96,97] have been shown to deliver electronic properties similar to those of periodic systems, opening the way to their systematic use, in a Time-Dependent Density Functional Theory (TD-DFT) framework in combination with localized atomic orbital (LAO) basis sets and hybrid exchange and correlation functionals, for the calculation of the optical properties of the dye@TiO_2 interfaces. This is, however, a peculiarity of the material, which yields size-independent electronic properties above a size of ca. 1-2 nm. The situation is completely different, for example, for ZnO and for related ZnX materials (with X= S, Se and Te), as well as for WO_3, which all exhibit strong quantum confinement effects.[98–100]

For the simulation of the dye-sensitized interface, the first step is to determine the adsorption mechanism of the dye onto the semiconductor, the nature and topology of the dye@semiconductor excited states, and the lining up of ground and excited state energy levels at the heterointerface. These properties, along with an estimate of the electronic coupling, constitute the fundamental parameters determining the electron injection and dye regeneration processes.[101–105] As it illustrated in Table 1, among the different types of anchoring functionalities, the ones employed in the most performant devices are the carboxylic groups, which can be grafted to the semiconductor surface by following a mono- or bi-dentate fashion.[106–108] The main drawback of cyanoacrylic and carboxylic

groups is their poor stability in water environments that has, for example, limited their utilization in dye-sensitized photoelectrocatalytic cells for water splitting.[109,110] On the other hand, phosphonic acid provides excellent anchoring stability, with an adsorption strength estimated to be approximately 80 times higher than that of the carboxylic acid, and negligible desorption in the presence of water.[11,111] Many alternative anchoring groups have been proposed and tested, such as hydroxyl,[112] silanes,[113] silatranes,[114] and hydroxamate[115] groups.

Dealing with solid/liquid interfaces, the inclusion of the solvent environment in the simulations is essential to reliably describe the photophysical behavior of the various cell components, especially if one wants to directly compare with experiments. The most common approach to take solvent effects into account at a low computational cost is to use implicit polarizable models, where the solvent is treated as continuum dielectric medium, being the Polarizable Continuum Models (PCM)[116] and the COnductor-like Screening Model (COSMO)[117] the most common implementations available in commercial quantum chemistry and solid state codes. Unfortunately, these approaches can only capture bulk solvation effects, while when specific solute-solvent interactions are supposed to take place at the interface, one needs to explicitly include the solvent in the simulations. A realistic description of explicit solvent effects and of its dynamics requires sufficiently long ab-initio Molecular Dynamics (AIMD)[108,118,119] or classical[120–122] MD simulations; hybrid Quantum/Molecular Mechanics (QM/MM) schemes, where the most relevant parts of the system (usually the solute and the first solvent layers) are described at the QM level, whereas the rest (the outer solvent layers) is treated classically, have been also largely applied.[123–125] Finally, concerning the dye/semiconductor/electrolyte

system interdependence, one should consider many important phenomena taking place at the dye/semiconductor, semiconductor/electrolyte, dye/electrolyte, dye/dye and dye/co-absorbent interfaces.[94]

2.2 Electronic Structure and optical properties of dyes in solution

DFT[126] and TD-DFT[127,128] are the most popular computational tools employed for the ground and excited state properties of DSSCs materials due to their excellent compromise between accuracy and computational cost. However, standard DFT functionals such as the ones based on the General Gradient Approximation (GGA) (i.e. PW91[129], PBE,[130] or BLYP[131]) usually fail in the description of the electronic structure and optical properties of dye sensitizers.[132,133] Pure DFT methodologies, indeed, present problems to recover the correct 1/R asymptotic behavior of the potential energy, yielding large underestimations for semiconductor band gaps, excited states with a significant long-range CT character and in the case of molecules with spatially-extended π systems.[134–137] While this error dramatically affects organic push-pull dyes and their interfaces with the semiconductor, [88,118,138,139] for TMCs the CT problem is limited to some extent by the substantial overlap of metal and ligand states characterizing the starting and arriving orbitals in MLCT excitations typical of these complexes. The use of opportunely tuned hybrid functionals, incorporating a variable amount of non-local Hartree-Fock (HF) exchange, partially corrects the wrong asymptotic behavior.[133,140–142] Other popular approaches are based on introducing an increasing fraction of HF exchange as the interelectronic separation increases; the long-range corrected (LC)

functionals,[143–146] the CAM-B3LYP[147] and ωB97XD[148] methods belong to this family of range-separated functionals. Finally it is worth mentioning a recent and promising new family of DFT functionals, namely the local hybrids,[149–154] whose tunability seems to be favorable for the description of hybrid DSSC interfaces.[139] In this approach different amounts of exact exchange are used at each point in space, thus allowing much more flexibility with respect to global hybrid and long-range corrected functionals.

Standard DFT methods also lack accuracy in treating long-range polarization effects that give rise to the van der Waals dispersion interactions, which, on the other hand, are properly taken into account by more expensive correlated *ab-initio* methodologies, such as second-order Møller-Plesset Perturbation Theory (MP2),[155] Coupled Cluster (CC)[156] or the Random Phase Approximation (RPA).[157] However, various correction schemes have been proposed to properly recover the dispersion interactions at the DFT level at a moderate computational cost.[158] These approaches are based on nonlocal density-based functionals, such as van der Waals (vdW-DF, vdW-DF2, vdW-DF3) [159] or Vydrov and Van Voorhis functionals (VV10)[160]; semiclassical C_6-based potentials, such as the Grimme's corrections (D2, D3),[161] Thatchenko-Scheffer (TS) models,[162] or Becke Johnson (BJ) damping functions[163]; and effective one-electron potentials, such as the semilocal meta-GGA Minnesota set of functionals (M06, M06-2X).[164]

Finally, another major drawback of TD-DFT methods is the well-known triplet (and multiplet) instability, which can be partially mitigated by resorting in the Tamm-Dancoff Approximation (TDA),[165] although it still may result in largely underestimated triplet excitation energies.[166] In the particular case of TMCs, where intersystem crossings (ISC)

involving several multiplicities often take place during the excited state dynamics,[167] the accurate estimation of such energies becomes crucial. It is well-known that pure exchange and correlation (xc) functionals tend to stabilize low-spin states, whereas the inclusion of HF exchange favors the high spin configurations.[168–170] Therefore, the reparameterization of standard hybrid DFT functionals with a slightly reduced amounts of HF exchange, as for instance, the modified B3LYP functional with a 15% of exchange (the so-called B3LYP*),[171] is one of the most popular strategies employed to model TMCs, as Fe(II) and Co(II) complexes.[172–175] In a similar way, the reparameterization of the short-range exact exchange in RSH functionals also provided accurate high and low spin state energy ($E_{HS/LS}$) values.[176] In the case of meta-GGA functionals, they have shown a good performance in the description of the optical properties of Fe complexes bearing strong ligand fields.[177] Furthermore, the so-called "double hybrid" functionals[178] have also shown to accurately estimate the relative $E_{HS/LS}$ energies.[179,180] Very recently, a cheaper computational alternative to these methods has been proposed by employing the Hubbard correction (DFT+U)[181] with a U-corrected density, which yielded to similar $E_{HS/LS}$ energies as the most accurate hybrid DFT approaches.[182] Finally it is worth to mention that the performance of TD-DFT to properly describe a large number of low energy quasi-degenerated states having a strong multiconfigurational nature and distinct CT characters, has revealed very system dependent.[183] In this context, more sophisticated computational approaches as, for instance, multiconfiguration pair DFT (MP-DFT)[184] or wavefunction methods such as CASPT2,[185] NEVPT2,[186], combined CASPT2/CC[187] or multireference CI[188], should be employed instead,[186,189] especially in those complexes with a more marked metal-ligand bond covalent character

which exhibit a huge dependence of the HF x-c fraction of the DFT functional chosen.[190,191]

The presence of heavy atoms used as metal centers in TMCs usually results in the appearance of relativistic effects affecting their electronic structure at different extent.[187,254] The splitting of the dye's energy levels and the population of certain forbidden triplet states originated by the coupling between the singlet and triplet states, spin orbit coupling (SOC), can heavily impact their opto-electronic response, especially in the lowest energy absorption region of the spectra. The full resolution of the Dirac Kohn Sham (DKS) equations is not computationally affordable for medium size systems as Ru(II) dyes and due to this, many different approximations to these equations have been developed during the last years. Among them, the most common approach to treat relativistic effects is the 2-component zero-order regular approximation (ZORA),[192,193] which is able to disentangle the scalar relativistic effects (SR) from the corrections associated to the inclusion of the spin−orbit coupling (SOC) operator. To understand the influence of the SOC between the lowest energy triplet and singlet states for a given molecular system, one can resort to a simple mono-electronic SOC model, where the oscillator strength of the lowest singlet-triplet excitations (f_{ST}) can be expressed as:

$$f_{ST} = \frac{\langle \Psi_T \rangle}{E_T - E_S} f_s \qquad (3)$$

Where Ψ_S/Ψ_T are the singlet/triplet wavefunctions, H_{SOC} is the spin-orbit coupling Hamiltonian, E_s/E_T are the singlet/triplet state energies, and f_S is the singlet oscillator strength. The matrix element at the numerator $\langle \Psi_S | H_{SOC} | \Psi_T \rangle$ represents the strength of the

coupling between the spin-free singlet and triplet states and it can be approximated by the amount of metal character in the metal-based Highest-Occupied Molecular orbital (HOMO) of the complex.[194] In this regard, with the aim of illustrating the implementation of these techniques in the modelling of TMCs, section 3 will provide a resume of the main theoretical studies dedicated to elucidate the influence of SOC in the properties of the Ru(II) complex dyes. Note that at this point, we will stick the discussion to the works done on Ru(II) and Os(II) dyes, since relativistic effects in Fe(II) complexes are expected to be very low in view of the low mass of its metal center.

2.3 Electronic Structure and optical properties of semiconductor materials and dye-sensitized interfaces

As discussed for the dyes, pure DFT functionals such as the ones based on the Local Density Approximation (LDA) usually lead to an underestimation of the experimental gaps of semiconductors as TiO_2[195], WO_3[196] or NiO.[197] This error can be corrected by adding a tuned fraction (10%-20%) of HF exact exchange in form of hybrid functionals.[198–201] As a matter of fact, however, hybrid functionals become an expensive method when modeling systems with large dimensions within a plane wave basis set. [202] In this regard, some computationally less expensive methods such as DFT+U[181] or DFT-1/2[203] have emerged during the last years as affordable solutions to overcome the DFT band gap issue in semiconductors as TiO_2. However, the need for an unbiased and accurate method enabling to fairly reproduce the electronic structure of both TiO_2 and the dye sensitizer has turned the attention to some many-body perturbation theory

(MBPT) methods such the ones based on the *GW* formalism,[204] which has recently become a prominent tool to investigate the interfacial energetics in DSSCs.[118,205,206] Concerning the dye@TiO_2 excited state properties, the large size of these systems clearly makes multiconfigurational correlated wavefunction methods, such as CASSCF, CC or CI, computationally prohibitive, and the reported calculations are limited to the interface with small TiO_2 clusters.[207] As a result, hybrid DFT functionals in combination with cluster models remain the most common tool to access to the dye@TiO_2 optical properties.[88] Nonetheless, the rapid development of MBPT approaches based on the combination of *GW* and the resolution of the Bethe Salpeter Equation[208,209] (*GW*/BSE) has recently allowed their implementation in the study of the excited state of these type of interfaces. [210,211] Still, the computational load needed to study realistic dye@TiO_2 models (owing hundreds or thousands of atoms) at the DFT level is still considerable, thus opening the door to the search of less expensive approaches such as Tight Binding (TB) models. Among these techniques, the TB method, whose parametrization is based on the second-order expansion of the DFT energies with respect to the charge density fluctuations (the so-called SCC-DFTB method),[212] is the most employed one. Indeed, the parametrization of Ti atoms to treat both bulk and molecular systems in DFTB[213] has allowed application of this approach to extended dye@TiO_2 interfaces, by providing realistic structures via geometrical relaxations[214,215] and AIMD simulations,[216–220] or by calculations of their excited state properties via its time-dependent implementation (TD-DFTB).[221]

The electronic structure of the dye@semiconductor interfaces can provide indications on the magnitude of the coupling between the states of the dye and the semiconductor, which determine the injection/recombination properties. The simplest method to estimate the

injection rates is based on the Newns-Anderson model,[222,223] which assumes that the coupling between the dye and semiconductor states is directly connected with the broadening of the Projected Density of States (PDOS) relative to the Lowest-Unoccupied Molecular Orbital (LUMO) of the sensitizer. An alternative still simple approach to estimate the recombination/injection ET reactions describes these phenomena as a non-adiabatic radiative process. Then the recombination/injection rates can be calculated as a function of two factors: the squared electronic coupling matrix element between the donor (dye's HOMO or LUMO) and the acceptor (semiconductor valence (VB) or conductance bands (CB)) and the Franck-Condon weighted Density of States (FCDS) which defines the probability of reaching a nuclear configuration where the donor–acceptor electronic states have the same energy, which in the case of semiconductors, reduces to a pure density of states ρ(E). Thus, by assuming a weak coupling, and resorting to the in the Fermi's Golden rule, as it has been proposed by Thoss and co-workers,[224] these rates can be estimated by employing the formula:

$$k_{inj} = \frac{2\pi}{\hbar} \sum_{k} |V_{dk}|^2 \rho(E_k) \tag{4}$$

Here k_{inj} represents the sum over the manifold of k acceptor states of interest and the product $|V_{dk}|^2\rho(E_k)$ defines the so-called probability distribution $\Gamma(E_k)$. A more refined method to investigate the interfacial dye@semiconductor ultrafast charge dynamics is based on the simulation of the laser-induced electron migration processes, where the laser-driven electronic wave packets are treated by means of the time-dependent many-body configuration interaction (TDCI) method.[225] Very interestingly, this approach has

allowed to evaluate the influence of the many-body interactions,[226] and to reach a real-time spatial representation[229] of the interfacial CT phenomena in dye@TiO_2 systems. Most of the methods commented above are applied to cluster models with a relatively medium size. For that reason, with the aim of evaluating the interfacial dye@TiO_2 electron transport phenomena in extended systems, one can resort to Non-Equilibrium Green Function (NEGF) Theory applied with the adequate boundary conditions.[227,228] More reliable information about the kinetics of the electron transfer phenomena occurring at the dye@TiO_2 interface can be obtained by means of quantum or non-adiabatic dynamics,[229,230] based on the time-dependent propagation of the electronic wavefunction, as obtained from semi-empirical Hamiltonians[231–233] or from the DFT orbitals,[234–236], combined with mixed-classical[237] or full quantum dynamics[238] simulations. On the same foot, much more expensive real-time propagation TD-DFT has been also emerged as a useful technique to access to the photoinduced electron transfer processes when combined with mixed classical quantum dynamics.[239,240]

2.4 Machine learning and semi-empirical methods applied to DSSCs

Finally, it is worthwhile to mention the recent attempts of integrating artificial intelligence (AI) and machine learning (ML) based approaches to the high-throughput screening of materials used as device components in DSSCs. This can be done by establishing reliable structure-property relationships obtained by the combination of accurate theoretical calculations and available experimental data. For instance, Ma *et al.* combined a database of 233 organic dyes with ML screening to discern eight potential organic dyes displaying

PCEs larger than 9% among 10000 possible candidates.[241] Ramanujam and co-workers designed a new ML route capable to predict novel high performant dye sensitizers, where 75% of them showed an improvement in PCE when compared to the reference dyes used to build the model.[242] One step further, Cooper *et al*. applied high-throughput screening to identify new materials displaying panchromatic optical absorption by selecting 6 combinations of co-absorbers (among 9431 dye candidates) which exhibited performances in the same order of magnitude as Ru(II) complexes.[243] On the same vain, these methodologies can also be employed to predict a given property that can be used as a descriptor of the device efficiency, thus allowing to identify which are the most important properties driving the cell performance. For the sake of illustration, Sutar *et al.* used ML to predict the best synthetic conditions to achieve ZnO electrodes with enhanced performances,[244] while Venkatraman *et al.* applied similar methods to identify which dye sensitizers are prone to undergo a larger red-shift when adsorbed on TiO_2 films.[245] All these results are a clear fingerprint of the huge potential of combining ML with large databases and high accurate calculations to assist the experimentalist to design and optimize of highly efficient DSSCs architectures.

3. Design rules for Ru(II) sensitizers: the role of spin-orbit coupling (SOC)

Due to their unsurpassed success, most of the theoretical works have been dedicated to the study of Ru(II) dyes (mainly N3 ($[Ru(dcbpyH_2)_2(NCS)_2]$, with $dcbpyH_2$=4,4‘-dicarboxy-2,2‘-bipyridine) and its salt N719. The first computational work was carried out in 1997 by Restmo *et al.,* who employed semi-empirical calculations to access to the electronic

structure of the best-performing N3 dye.[246] Only in the early 2000's the pioneering works on the excited state properties of Ru(II) sensitizers (N3 and the related salt N719) based on TD-DFT calculations appeared in the literature.[247,248] Standard hybrid functionals such as PBE0 and B3LYP gave accurate results in the description of the three main bands, centered at 2.6, 3.4 and 4.2 eV, dominating the absorption spectrum of the N3 dye (see Figure 3 left). The inclusion of solvent effects, even only by an implicit solvation model, was proved to be mandatory to describe the optoelectronic properties of this class of Ru based dyes, and the adopted methodology was able to reproduce the 0.2 eV red-shift and the appearance of a low energy absorption shoulder experimented by the N3 spectrum when substituting the -CNS ligands by Cl- groups (see Figure 3 right).[249] Moreover, the experimental solvatochromism shown by the N3 sensitizer going from ethanol to water was accurately predicted and related to a decreased dipole moment in the excited state with respect to the ground state, which translates into a higher stabilization of the ground state in solvents of increasing polarity.[247] The following studies on Ru based complexes have confirmed the importance of taking into account the surrounding effects.[250–253] From the analysis of the TD-DFT calculations shown in Figure 3, the two bands appearing in the Vis region were assigned to mixed Ru−NCS/Cl to bipyridine−π* transitions, whereas the band in the UV region was attributed to local bipyridine π→π* transitions. Very interestingly, the electron withdrawing nature of the -NCS/-Cl moieties localizes the photogenerated holes around this groups and, due to this, the lowest absorption bands of these complexes can be considered as NCS/Cl ligand-to-bipyridine transitions rather than typical MLCT states. This feature is at the origin of the efficient intramolecular charge separation and the correct flow of charge towards the ligands bearing the carboxylic

anchoring groups, thus making the N3 the system of reference to reach performant DSSCs devices.

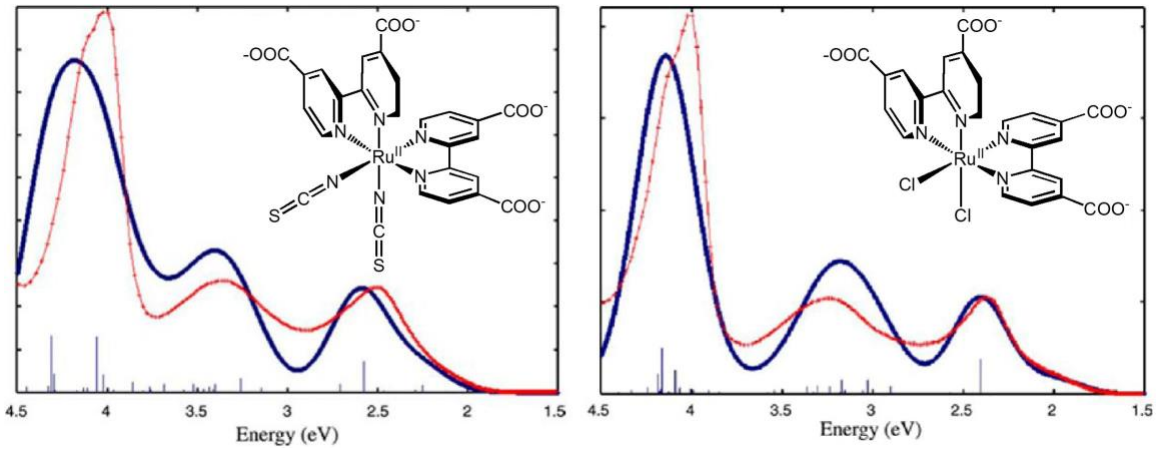

Figure 3. Comparison of the TD-DFT simulated (blue) and experimental (red lines) spectra for the *cis*-[Ru(4,4′-COO-2,2′-bpy)$_2$(X)$_2$]$^{4-}$, X = NCS (left) and Cl (right) dyes in water solution. The chemical structures for both dyes are represented inset. Figure adapted with permission from ref. [249] Copyright 2005 Elsevier.

The computational strategy set up for N3 was extended to its salt N719 and to the amphiphilic heteroleptic [Ru(dcbpyH$_2$)(tdbpy)(NCS)$_2$], N621 dye (dcbpyH$_2$ = 4,4‘-dicarboxy-2,2‘-bipyridine, tdbpy = 4,4‘-tridecyl-2,2‘-bipyridine) to evaluate the effect of protonation and counterions on the electronic structure, redox and optical properties of the investigated dyes.[254] The good agreement between the simulated properties and the experimental data has allowed the use of DFT and TD-DFT calculations to screen new Ru-polypyridyl dyes before moving on to synthesis. Moreover, through computational modelling, structure-electronic/optical properties relationships have been established thus providing design rules to extend the solar light absorption towards the nIR. As it is illustrated in Figure 3, the absorption features of standard Ru(II) complexes such as N719

or N3 are reproduced by computing their singlet states at the TD-DFT level. These dyes display their lowest energy absorption at 450 and 530 nm for their -CNS and -Cl ligand equivalents respectively, what in a certain manner limits their capability to absorb red photons in the nIR region from solar light.[255] With the objective of red-shifting the absorption of Ru(II) complex, new dyes showing a panchromatic absorption in the nIR-Vis region appeared in the literature. In this respect, the first one of these compounds was the so called black dye (BD), which was synthetized by employing one single terpyridine (tpy) and three -CNS ligands (see Figure 4), and it showed a red-shifted absorption centered at 610 nm.[255] Later on, Segawa and coworkers developed a new panchromatic dye (DX1) by substituting one of the -CNS ligand of BD by a phosphine coordinated group (see Figure 4). As a result, this complex presents a lower energy absorption band up to ca. 800 nm contrary to the previously reported Ru(II) dye bands, attributed to singlet to triplet transitions.[256] It is well known SOC has a small impact in determining the absorption spectra of the investigated ruthenium complexes, indeed, SOC is generally considered an atomic property related to heaviest elements, nevertheless as a general trend the SOC induces in this class of compounds a slightly red-shifted absorption tail, corresponding to the contribution of singlet-triplet excitations, with a concomitant slight reduction of the more intense singlet-singlet transitions giving rise to the absorption maximum region, in line with expectations. With the aim of favoring the direct singlet-to-triplet transitions, similar dyes to DX1 owing modified phosphine groups bearing weaker ligand fields (DX2 and DX3)[257] and (DX4-DX6)[258] were synthetized and characterized (Figure 4). Due to their enhanced spin-orbit coupling interaction, the lowest absorption features of this class of TMC sensitizers were shifted up to 1000 nm.[257,258] In view of these experimental

evidences, the treatment of relativistic effects became a major issue for the modelling of panchromatic dyes.[259]

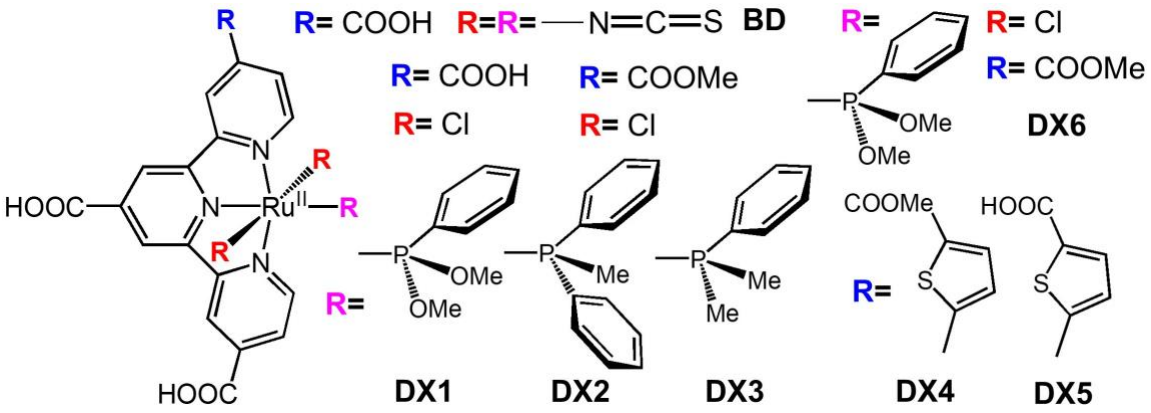

Figure 4. Chemical structures of the panchromatic Ru(II) dye complexes based on tpy ligands.

The first work tackling the impact of SOC in the opto-electronic response of Ru(II) dye sensitizers was conducted by Daul *et al*, which analyzed the nature of MLCT states of the prototypical $[Ru(bpy)_3]^{2+}$ complexes, and pointed to the mixing of their singlet and triplet states as the origin of the degeneracy the MLCT absorption bands.[260] However, this degeneracy was further measured experimentally by quantifying the HOMOs splitting of the $[M(bpy)_3]^{2+}$ (M=Fe, Ru, Os) dyes, which indeed, was found only significant for M=Os, whereas M=Ru, Fe dyes showed a low energy splitting below 0.3 eV.[261] This low influence of the relativistic effects in the $[Ru(bpy)_3]^{2+}$ electronic structure was confirmed by some of us and extrapolated to N3 by comparing the opto-electronic properties of both dyes calculated at the SR and SOC levels of theory.[262] Regarding their electronic properties, only a small destabilization of 0.1 eV was found for the HOMOs without

implying a modification in the orbitals delocalization upon including SOC. In the case of the absorption features, SOC inclusion induced only a small intensity decrease and a red-shift in the lower-energy region of the calculated spectrum (see Figure 5-a). In spite of this, the small but sizable differences in the relative position of the singlet and triplet states of $[Ru(bpy)_3]^{2+}$ and N3, pointed to the possibility of enhancing the singlet-triplet coupling via ligand modification.[262] In this regard, in view of the remarkable singlet-triplet interactions reported for the panchromatic dyes BD and DX1, which enabled to build high performant DSSCs devices (~11.4% for both dyes),[256,263] some of us proceeded to evaluate the impact of relativistic effects in the photovoltaic behavior of BD and DX1.[264] The larger HOMO energy splitting observed in DX1 when compared with BD, is attributed to their different electronic structure where the HOMO and HOMO−1 (of d_{xy} and d_{xz} character in DX1) are switched in BD and displayed a reduced amount of metal character. Due to this, the calculated spectrum of BD was not modified upon inclusion of SOC (Figure 5-b), whereas for DX1 it promoted a small shift absorption maximum (~0.05 eV), and more importantly, a broadening of the MLCT band prompted by this energy splitting (see Figure 5-c). As a result, the SOC-induced spectral broadening slightly enhances the light-harvesting efficiency, and it consequently contributes additional photocurrent (~2.3 mA/cm^2, 32% of increase) in DX1-sensitized DSSCs (Figure 5-d).[264] In view of the positive impact of singlet-triplet couplings in the device performance, further theoretical studies were carried out with the aim of boosting relativistic effects via chemical engineering of the ligands. For instance, Kanno *et al* showed that the substitution of the -CNS and -Cl ligands in N3 and DX1 by iodine groups can be employed to increase the strength of SOC due to the heavier mass of this atom.[265] On the same vain, Mishima *et*

al found very small modifications of the absorption features of DX1 by changing the substituents of the phosphine ligand, and confirmed that relativistic effects are higher for these dyes with respect BD due to the higher covalent character of these ligands.[255] Notably, TD-DFT SOC calculations showed that the large red-shifted absorption observed in DX3 is originated by the reduced energy difference between the two lowest energy triplet states, resulting in a higher coupling with the singlet states with respect to DX1 and DX2.[257] Finally, the introduction of a conjugated thiophene group coupled to the tpy ligand for DX4 and DX5 yielded to enhanced oscillator strengths for singlet-singlet and singlet-triplet transition, whereas the extent of singlet-triplet couplings remained unaltered.[258] Overall, despite DX3 represents the upper limit for the red-shifted absorption in panchromatic Ru(II) complexes, relativistic effects can be significantly boosted by employing heavier atoms as metal centers as for instance Os.[259,266,267] In spite of their promising red-shifted absorption, the use of such as heavy atoms should be somehow limited due to the toxicity and scarcity issues commented above.

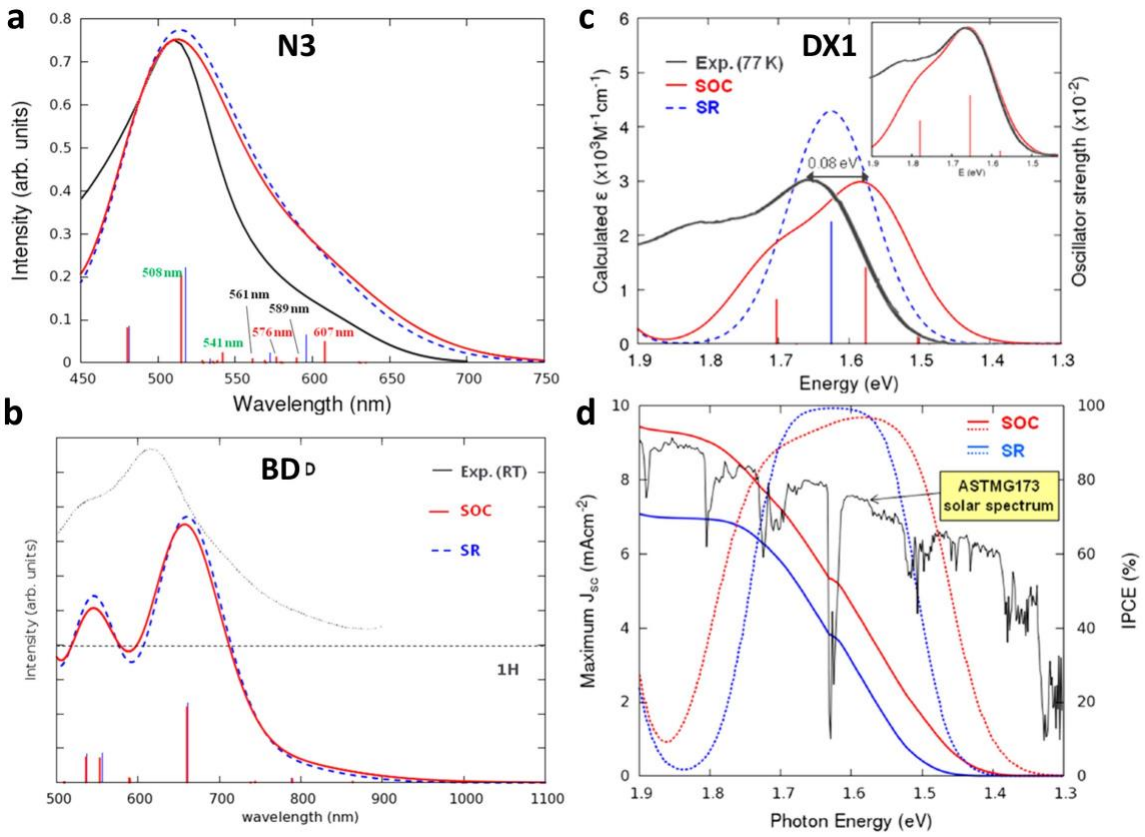

Figure 5. Simulated absorption spectra calculated at the SR (blue) and SOC (red) levels of theory, together with their respective experimental spectra (black lines) for the a) N3, b) BD and c) DX1 dyes; and d) maximum J_{SC} (mA/cm^2, dotted lines) and IPCE curve (%, full lines) for DX1, as computed at the SR (blue) and SOC (red) levels, against the ASTMG173 solar spectrum (black line). Images adapted with permission from ref. [262] and [264] Copyright 2014 American Chemical Society.

4. Modeling the photophysics of Fe(II) metal complexes: tools and findings

As discussed above, the success of Ru-based complexes in DSSCs and other applications is essentially due to their long-lived triplet ^{3}MLCT states, up to microsecond timescales.

As already mentioned, polypyridyl Fe(II) complexes, having their six valence electrons paired in the lowest energy metal centered *d* orbitals, experience ultrafast (ca. 50 fs) deactivation to low-lying metal-centered (MC) states, via the triplet ^{3}MC and ultimately the quintuplet $^5T_2$ states,[268,269] thus impeding any efficient utilization of photoinduced electron transfer reactions.

As it is exemplified in Figure 6-a, the main difference in the photophysics of the Ru(II) vs Fe(II) complexes lies in the inversion of the MLCT and MC states energetics, that originates from the fundamental electronic structure features of the first-row metals.[268] The absence of a radial nodal plane at a large distance from the nucleus for n=3 and l=2 (3d) wavefunctions causes a reduced screening of the nuclear charge and thus a "contraction" of the 3d orbitals.[70] This, in turn, results in a decreased orbital overlap between the metal and the ligands and, thus, in a lowered ligand-field strength. This intrinsic weaker ligand-field splitting in Fe(II)-polypyridyl octahedral complexes, compared to the Ru(II) analogous, yields a stabilization of the MC states in the formers, whereas the MLCT states, whose energy is related to the metal oxidation potential, remains essentially unchanged. Due to the distinct relaxation pathways that Fe(II) complexes can follow from the MLCT to the MC states, their photophysics is quite intricate and usually involves many possible cascade intersystem crossings (ISCs) (see Figure 6-b).[270] Many different strategies have been pursued to increase the lifetime of the Fe(II) complexes MLCT states featuring the destabilization of the MC states by increasing the ligand strengths via chemical functionalization with strong σ-donating, [77,78,83] combined σ- and π-donating,[271,272] σ-donating and π-accepting groups;[273,274] or the population

of the ^{5}MLCT state as obtained by further decreasing the ligand field to achieve a high-spin ground state (^{5}MC) in highly strained complex structures.[275,276]

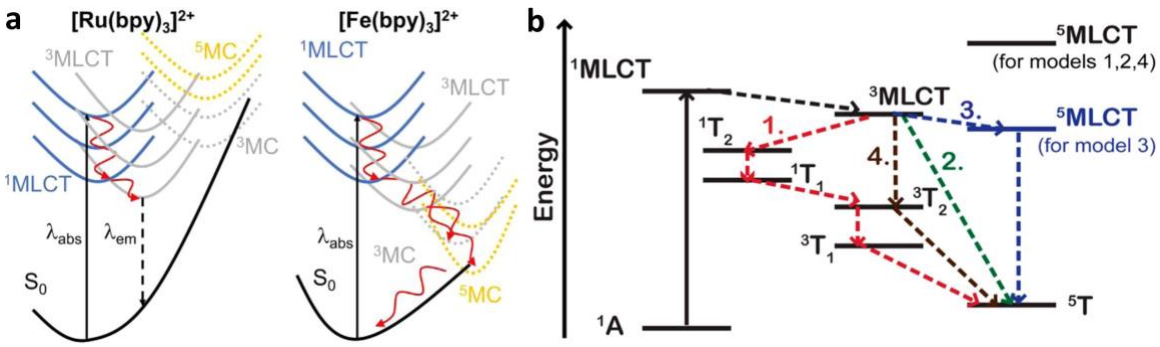

Figure 6. a) Schematic representation of the MLCT states decays of $[Ru(bpy)_3]^{2+}$ and $[Fe(bpy)_3]^{2+}$ complexes, where solid/dashed black arrows are used to indicate light absorption/emission ($\lambda_{abs}/\lambda_{em}$) mechanisms, and red curly arrows depict vibrational relaxation and non-adiabatic population processes. Note that MLCT and MC surfaces have been represented with continuous and dotted lines, respectively. Image adapted with permission from ref. [277] Copyright 2019 Wiley-VHC; b) energy diagram representation of the distinct models for ^{1}MLCT→^{5}MC(^{5}T) relaxation pathways proposed in the literature. Image adapted with permission from ref. [271] Copyright 2015 American Chemical Society.

In this context, a computational set up able to track accurately the relative energies and relaxation decays of the MLCT and MC states via potential energy surface (PES) curves has been at heart of the recent developments of Fe(II) complex for dye-sensitized technologies.[277] Nonetheless, this is not a trivial task, since one needs to track the

different electronic, structural and environmental effects governing the excited states relaxation pathways. The simplest computational approach employed to this purpose is based on the computation of the equilibrium (adiabatic) energies for the MLCT and MC states in their triplet and quintuplet geometries.[272] Calculations of adiabatic energy levels, however, does not give information concerning the crossing points between the involved excited states and the associated energy barriers; this requires the characterization of the corresponding PESs in order to identify the different non-adiabatic events that lead the decay pathways. A computationally affordable and conceptually simple approximation to the PESs can be obtained by fitting the energies and the most relevant vibrational frequencies of the optimized excited states with harmonic functions.[278,279] This technique was employed by Warnmark and co-workers to shed light on the origin of the long-lived ^{3}MLCT states (528 ps) observed for an homoleptic Fe(II) complex bearing bidentate NHC ligands. The authors attributed this exceptionally long lifetime to the presence of a relatively high energetic barrier (0.12 eV) that should be overcome to access to the conical intersection with the ^{3}MC state, whose minimum lies lower in energy with respect to the ^{3}MLCT minimum (see Figure 7-a).[280] Unfortunately, for certain cases the PESs estimated by this method are not realistic, especially for those structures lying far from the Frank-Condon region or in those systems where the relaxation decays are not following a harmonic shape. Alternatively, PESs can be explicitly calculated by linearly interpolating one or several coordinates relevant for the photoprocess.[281] This approach can deliver accurate enough energy profiles of the states of interest, rough (upper bound) estimate of crossing points and reliable insights into the operative decay mechanisms and their specific competition. In the particular case of Fe complexes, the metal-ligand

distances and ligand-metal-ligand angles represent the main geometrical parameters governing their excited state energies,[282] due to the antibonding character of the orbitals populating the ^{3}MC and ^{5}MC states. The energy scans for these two coordinates has allowed to study the relaxation pathways of some Fe(II) complexes via the construction of their respective 2D PES curves, demonstrating that ISCs in $[Fe(terpy)_2]^{2+}$ cannot be described by using a single configuration coordinate.[283] For getting more accurate PES curves including a larger number of molecular motions, one can implement certain interpolation algorithms to elucidate the energy paths between two given optimized structures, as for instance, the high and low spin geometries. In this regard, Jakubikova and co-workers employed a sparse grid interpolation algorithm to get an approximation of the energy paths between the ground and the ^{1,3}MLCT and ^{3,5}MC states of a terpyridine ligand complex $[Fe(tpy)_2]^{2+}$ ISCs. This work pointed to the relative rock motion of one of the ligands Θ as the main geometrical coordinate dictating the crossing points between the studied states (see Figure 7-b).[271]

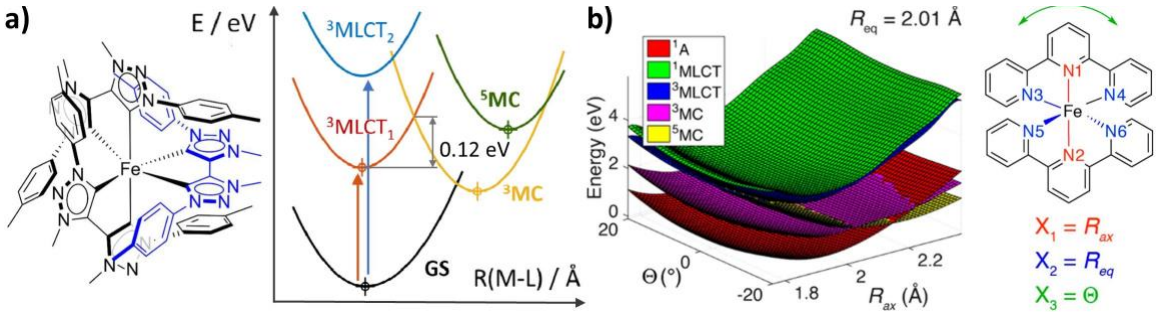

Figure 7. a) Scheme of the parabolic energy surfaces for the main states of the $[Fe(btz)_3]^{2+}$ depicted on the left part of the image, as a function of its M-L distances; and b) PESs for the ^{1}A, ^{1,3}MLCT, and ^{3,5}MC for the $[Fe(tpy)_2]^{2+}$ complex as a function of the R_{ax} and Θ

coordinates, while keeping fixed the value of R_{eq} = 2.01 Å; as they are represented in the image on the right part. All energies are relative to the interpolated minimum of the ^{1}A state. Images adapted with permission from refs. [280] and [271] Copyright 2015 and 2018 American Chemical Society; for panels a) and b) respectively,

However, when reconstructing PESs by interpolations between different minima, each point is not necessarily an energy minimum and thus the calculated pathway is not the lowest energy route. A more refined, and computationally onerous, approach consists in the calculation of minimum energy paths (MEPs), where any point represents a minimum in all directions perpendicular to the path.[275] In this context, different computational schemes have been implemented. One of these techniques consists in considering the intrinsic reaction coordinate (IRC) which estimates the transition states (TSs) between two local minima (even with different multiplicity) by resorting for instance to analytic nuclear gradients.[269,[284] Some of us also employed this approach to elucidate the effect of the fac/mer isomerism on the photophysics of a bidentate pyridyl−carbene Fe(II) complex.[285,286] We reported the full DFT PES landscape for both isomers by computing the MEPs from the ^{3}MLCT to ^{3}MC minima adopting the IRC algorithm (Figure 8). Transient absorption spectroscopy (TAS) measurements suggested that the ^{3}MLCT decay for both fac and mer isomers proceeds with a parallel two-state mechanism: a fast component (2–3 ps and 3–4 for ps mer and fac, respectively) and a slow one (15–20 ps). In addition to this small difference in the fast component, the two isomers also showed different branching ratio, and hence the probability, of the two decay pathways. Indeed,

while for the fac arrangement the fast/slow branching ratio is of 57 %, for the mer isomer it accounts for 87 %.

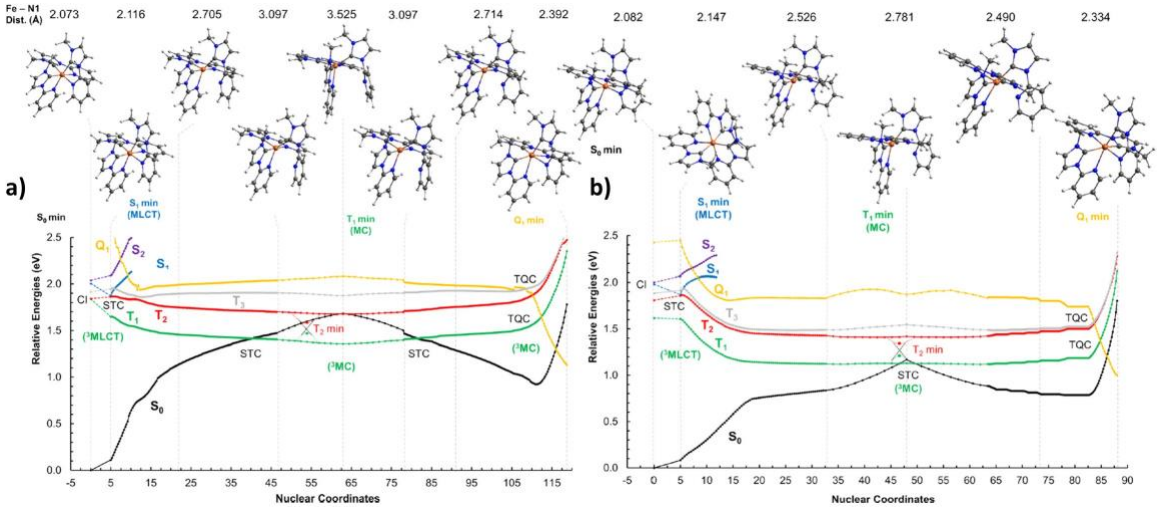

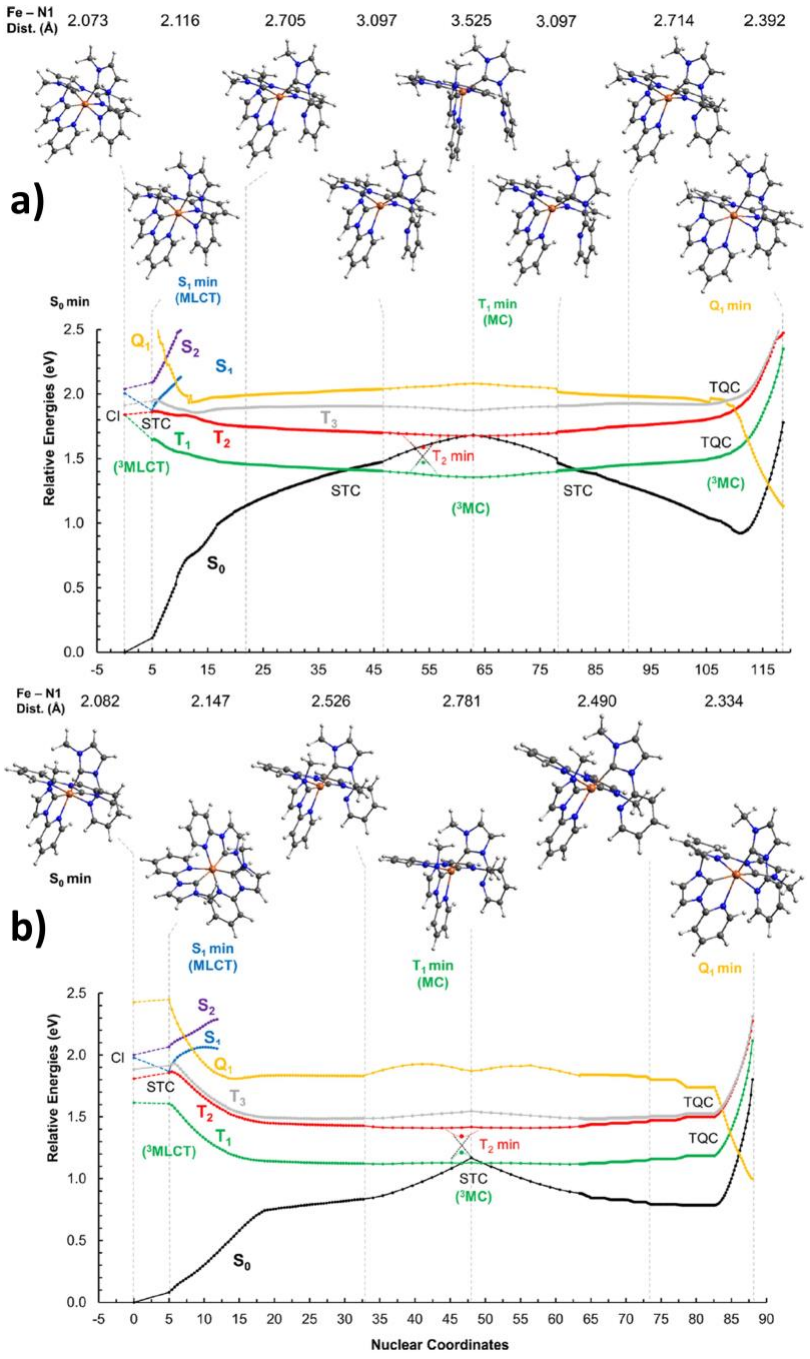

Figure 8. Lowest-lying singlet, triplet and quintet PESs of a) fac-Fe-NHC and b) mer-Fe-NHC. Arbitrary nuclear coordinate values are used to label the structures obtained along the decay path. CI = conical intersection, STC = singlet–triplet crossing, TQC = triplet–quintet crossing. Image adapted with permission from ref. [287] Copyright 2018 American Chemical Society.

In both isomers, based on the calculated PESs, the fast component was ascribed to the decay of the T_2 state (T_2/S_0 crossing points), whereas the slow component was assigned to the deactivation of the T_1 state (T_1/S_0 crossing point). On the other hand, the differences in the branching ratio of the two components was interpreted based on the steeper MEP computed for the mer isomer (see Figure 8-b) with respect to that of the fac arrangement (see Figure 8-a).

However, IRC algorithms still present some limitations due to the fact that optimizing TSs in the excited state can be rather problematic since, in Fe(II) complexes as in many other systems, the reaction coordinate is often complex and involves coupled variations in bond lengths, angles and dihedrals and the accuracy is highly dependent on the initial guess used as starting geometry. To overcome this problem, the Nudged Elastic Band (NEB) method[287] optimizes a number of intermediate images along the reaction path between the reactant and the product. Each image finds the lowest energy possible while maintaining equal spacing to neighboring images by adding spring forces along the band between images and by projecting out the component of the force due to the potential perpendicular to the band.[287] This methodology accounted for 0.2 eV the energy barrier between the ^{3}MLCT and ^{3}MC states in $[Fe(tpy)_2]^{2+}$ complexes bearing cyclometallating ligands with degenerate triplet states. Such a high energy barrier may trap the system in the initially populated ^{3}MLCT state. Indeed, the authors suggested a ^{3}MLCT⇌^{3}MC equilibrium process highly influenced by the deactivation of the ^{3}MC state via its crossing

with the ground state, requiring a barrier of 0.18 eV, also depending on the SOC magnitude between the ^{3}MC and the S_0 states. [272]

Before closing this section it is noteworthy to mention the attempts made to extract direct information on the excited state lifetime by theoretically investigating the excited relaxation pathways, through excited state quantum dynamics simulations.[73] In this direction, Papai and coworkers performed quantum wavepacket dynamics simulations on top of PESs built as solutions of a spin-vibronic Hamiltonian describing the non-adiabatic vibronic coupling.[288] This work elucidated the excited state relaxation process in a $[Fe(bmip)_2]^{2+}$ (bmip=2,6-bis(3-methyl-imidazole-1-ylidene-pyridine) complex: ^{1}MLCT→^{3}MLCT relaxation occurs within 100 fs, followed by population of the ^{3}MC states. The ^{3}MLCT-^{3}MC deactivation is slower than in $[Fe(bpy)_3]^{2+}$ due to a high excited state barrier and modest spin-orbit coupling along two dominant Fe−L breathing modes modulating the Fe−N and Fe−C bond distances.[289] The same approach showed that the substitution of the methyl moieties of this complex by tert-butyl groups promotes the stabilization of the ^{1}MC states, thus enabling their population from the ^{1,3}MLCT states close to the Frank-Condon geometry.[172] The use of on-the-fly non-adiabatic dynamics is computationally prohibitive when dealing with TMCs, characterized by a high density of quasi-degenerate and strongly coupled states that could be populated. Moreover, one needs to propagate a large number of trajectories to achieve a statistically significant representation of the process. Recently the Gonzalez's group reported state-hopping dynamics simulations with a linear vibronic coupling model to understand the first steps of the excited state relaxation in a Fe−NHC complex,[290] and it evidenced the ultrafast population (50 fs) of its triplet states upon irradiation with a small component of MC

character which lead to non-radiative recombination.[291] Although no direct comparison with experiments is provided in this work, it nicely shows the potentiality of the non-adiabatic dynamics approach to shed light on the photophysics of TMCs.

5. Interfacial properties of Fe-NHC sensitized TiO_2

The first photovoltaic characterization of the Fe(II)-NHC complex C1 (Figure 2) was reported by Gros end co-workers in 2015 with the first realization of iron-based DSSCs.[79] Despite their relatively long lifetimes and suitable energetic alignments with both the TiO_2 CB edge and the I^-/I_3^- oxidation potential, the homoleptic Fe(II)-NHC complex yielded extremely low photocurrent and photovoltage, resulting in weak power conversion efficiencies (0.13%).[79] It is important to highlight here that besides a sufficiently long ^{1,3}MLCT lifetime, being mandatory for injecting electrons into the TiO_2 CB, the measured overall cell efficiency finally depends on the specific properties of the dye-sensitized interface (adsorption configuration, electronic coupling, charge generation, charge recombination etc.). On the other hand, a subsequent work by Wärnmark and co-workers[80] claimed a record injection efficiency, almost unitary, for the same C1 complex, attributing the low photovoltaic performances reported in Ref.[79] to a fast recombination of the injected electron with the oxidized dye. In view of this, after the first proof of the practical use of Fe sensitizers in solar energy technologies, the main strategies followed to boost their device efficiencies have followed two different directions: the chemical engineering of the dye structure[26–28,279,292,293], and the optimization of the electrolyte composition.[25,26,294,295]

Before analyzing the interfacial dye@TiO_2 properties of Ru(II) vs Fe(II) complexes we will briefly discuss the nature of their lowest energy absorption features. Regarding the Fe(II)-NHC complexes, the heteroleptic dye, ARM13, displays two absorptions bands in the Vis region centered at 461 nm and 385 nm, originated from MLCT transitions toward the anchoring ligand; and a local $\pi \rightarrow \pi^*$ transitions of the unanchored ligand, respectively. Unfortunately, due to the low donor character of the Fe(II) metal center, holes start to delocalize around the unanchored ligand, thus making the charge separation less efficient due to its local character and facilitating electron recombination. The inclusion of a second carboxylic group in the homoleptic dye C1 induces in a small red-shift of the absorption bands and an increase in the absorption intensity (see Figure 9 left). Due to their symmetry the hole/electron contributions of the two ligands to the MLCT state are equal (Figure 9). Nonetheless, this symmetry will be broken upon the deprotonation of the ligand which is attached to the surface. Notably, for the deprotonated C1 (called C1(D) in the following) its lowest energy MLCT transition is pointing towards the protonated ligand and therefore, in the case of being populated, this will yield to a CT moving in the opposite direction to the charge injection into the TiO_2 surface. Interestingly, the insertion of π-conjugated bridges (i.e. a phenylene or thiophene moieties) between the carboxylic group and its correspondent NHC ligand in the heteroleptic dyes makes the MLCT states acquiring a local π-π character around these moieties, resulting thus detrimental for the charge separation due to the lower extent of electron delocalization around the carboxylic anchoring groups (16% vs 7-8% for ARM13 and their π-conjugated anchoring ligand analogues).[26] Finally, the functionalization of ARM13 with an electron donor moiety (as

in ARM130 or FeCD) resulted in a considerable enhancement of the absorption band harvesting, while on the other hand, the nature of the MLCT transition remained unaltered (Figure 9).

Overall, the different natures of the lowest energy MLCT bands of the Fe (II) vs Ru(II) dyes in terms of charge separation and directionality already provides some important hints to explain the superior performance reached by the latter complexes, but let's consider now their interface with TiO_2 and some possible strategies to have been proposed to mitigate these drawbacks.

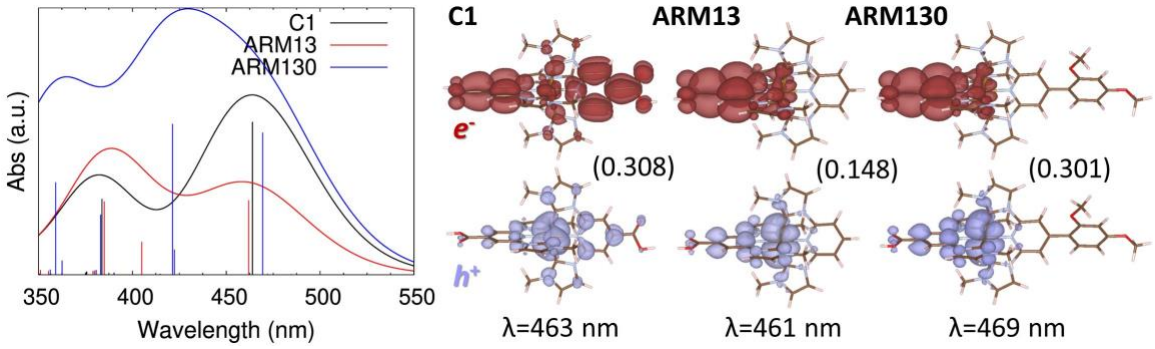

Figure 9. Simulated absorption spectra (left) and Natural Transition Orbitals (NTOs)[277] for the most prominent lowest energy states (right) for C1, ARM13 and ARM130, as calculated at the TD-B3LYP*/6-311G** level of theory with the CPCM to treat the methanol solvent environment. The absorption wavelengths and oscillator strengths for each state represented in the NTOs are also reported. The isovalue used to represent the isodensity plots was set to 0.02 a.u.

The first work dealing with the interface of Ru(II) complex with TiO_2 was reported in 2005 by Person and co-workers, which studied the absorption of N3 attached to a $(TiO_2)_{38}$ cluster at the TD-DFT level, and predicted a MLCT injection time which amounted to 10 fs.[296] During the following years, many works appeared in the literature with the aim of discerning which are the most stable anchoring binding modes for that dye and their relation with the injection rates, and reported injection lifetimes which ranged from few to 100 fs depending on the anchoring mode.[86,297,298] In one of these works, some of us reported a TD-DFT study of the N3 dye adsorbed on a $(TiO_2)_{82}$ cluster with three carboxylic moieties attached to the semiconductor (one bidentate and two monodentate binding modes).[88] The computed absorption spectrum in the lowest energy region was nicely reproducing the experimental one (see Figure 10-a), with the most prominent transition (the one with the largest oscillator strength) corresponding to the S_{18} state (555 nm). By looking at the charge density difference plot between S_0 and S_{18} depicted in Figure 10-b it is possible to appreciate how, apart from the adequate CT directionality and separation, the excited electrons are largely delocalized along the TiO_2 surface, what is a clear fingerprint for a direct ultrafast injection process. Focusing now on the interfacial energetic alignment represented in Figure 10-c, the HOMO of the dye in the N3@TiO_2 lies far from the CB/VB of TiO_2, thus avoiding undesired recombination processes, whereas its LUMO lies about 0.3 eV above the CB edge of TiO_2, assuring the correct thermodynamics of the electron injection and its position in a densely populated region of TiO_2 states yields to a strong coupling with the semiconductor.[88] It is noteworthy to highlight that in this paragraph we focused only on the electronic and absorption properties of the N3@TiO_2 interface as a illustrative way to discern the main differences with respect

to the Fe(II) dye@TiO_2 systems, whereas many other works have been dedicated to the interfaces of another types of Ru(II) dyes with TiO_2 (such as BD)[299–301] and resulted in similar results as the ones observed with N3.

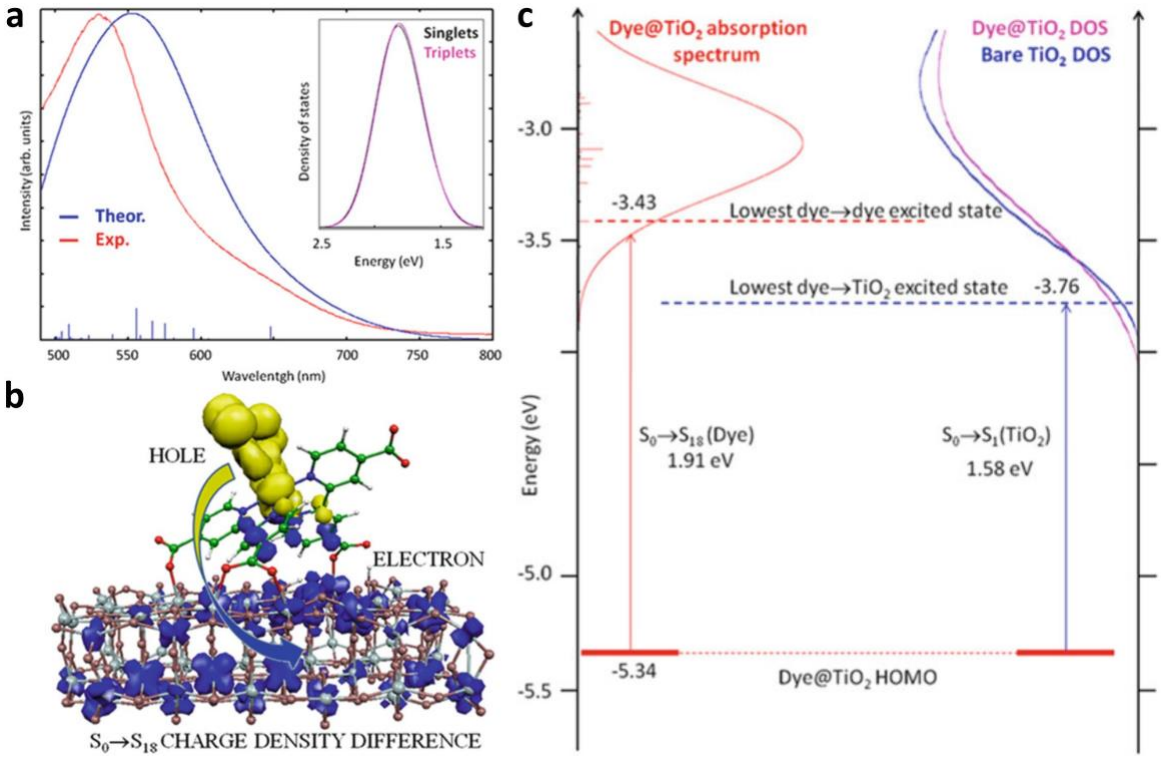

Figure 10. a) Normalized simulated (blue) and experimental (red) absorption spectra of N719 on TiO_2, with the inset representing its calculated density of singlet (black) and triplet (magenta) excited states; b) $S_0 \rightarrow S_{18}$ charge density difference between plot of the N719@TiO_2 system where blue/yellow colors are used to represent the photogenerated electron/hole densities; c) energetic level alignment of the ground and excited states for the N719@TiO_2 system (left) and calculated DOS of the interacting and isolated TiO_2 cluster (right). Image adapted with permission from ref. [89] Copyright 2013 American Chemical Society.

The first theoretical work investigating the impact of the cyclometallation of the pyridine ligands in the MLCT lifetimes and injection rates of the $[Fe(tpy)_2]^{2+}$ complexes was reported by Jakubikova and co-workers.[302] They found that despite the use of carbene ligands assists the stabilization of the ^{1}MLCT states, they can be detrimental for the injection due to the localization of the electron density around the carbene groups instead of the carboxylic anchoring moieties, resulting in injection times in the order of 100 fs.[302] This work represented the first evidence of the suitability of employing NHC ligand Fe(II) complexes for photovoltaic applications. In this regard, Fredin and co-workers studied the electronic structure of the heteroleptic NHC complex interface (ARM13@TiO_2) showing that NHC complexes exhibit a suitable energy level alignment and LUMO couplings with respect to the TiO_2 CB, yielding electron injection rates of about 100 fs, as estimated on the basis of a Newns-Anderson model.[279] Nonetheless, these calculations were not able to fully rationalize the low device efficiencies firstly reported when employing this dye as sensitizer, and the main question related with the fast recombination occurring at the semiconductor interface were still unclear.[303] In this context, some of us investigated the interface with TiO_2 for the prototype homoleptic and heteroleptic NHC Fe(II) complex dyes (C1 and ARM13).[292] Figure 11 presents the PDOS along with the molecular and semiconductor parts of the dye@TiO_2 interface. All considered complexes remained tilted on the semiconductor surface, forming an angle with respect to the surface plane of approximately 45º, which was consistent with the previous studies.[279] The energetic alignment for the three complexes resembled to the one schematized in Figure 10-c, with the dye HOMOs lying above the VB and the LUMO above the TiO_2 CB edge. In the case of the HOMOs, despite these levels are mainly

delocalized over the molecular backbone, they also exhibit a considerable mixing with the TiO_2 VB states (~30-50%), as it is evidenced by the tail of the TiO_2 VB extending through the dye's HOMOs PDOS, which can be originated by the close contact between the tilted dyes and the surface. This high HOMO coupling with both CB and VB states leads to high recombination rates (in the ns or ps timescale) and thus to an inefficient charge injection/recombination at the interface. On the other hand, the energetics and spatial distribution of the unoccupied molecular states differ as a function of the dye. In the case of C1, the dye's LUMO is essentially not coupled with the TiO_2 CB states (with 93% localized on the dye backbone), whereas the LUMO+1 exhibits a strong coupling with the semiconductor (2% dye's contribution). As a result, the primary charge transfer channel from the lowest MLCT state appears to point towards the opposite direction to the charge injection into the semiconductor. Similar PDOS features were also observed for ARM13, thus demonstrating that the use of heteroleptic dyes permits to obtain the correct CT directionality. The calculated injection times for the strongly coupled LUMO levels were in the few fs timescale, thus showing an ultrafast injection process, in analogous way as the one reported in Ru(II) complex dyes.[292]

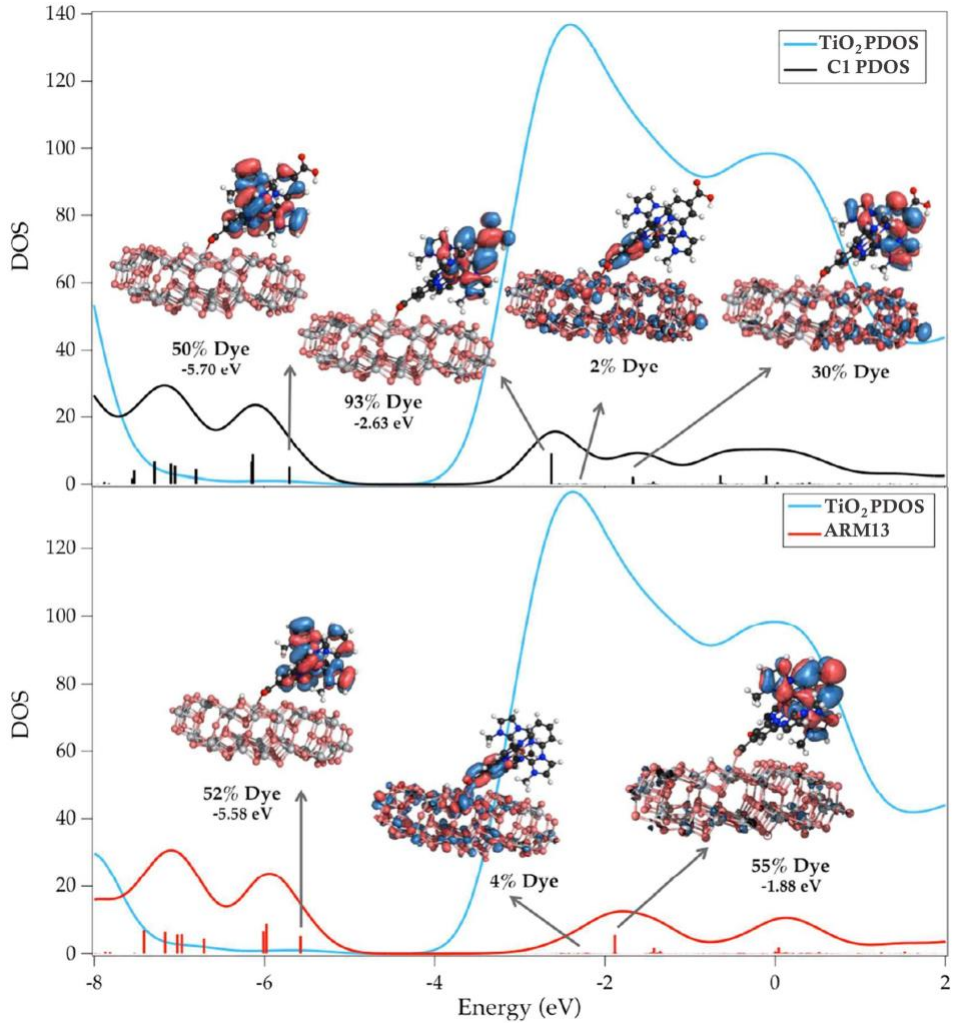

Figure 11. PDOS over the dyes (black/red colors for C1/ARM13) and TiO_2 surface (blue), and main dye's Mos isodensity plots for the C1@TiO_2 and ARM13@TiO_2 systems. The corresponding percentage of dye's delocalization and energies in eV are reported for each MO plot. Vertical bars intensities represent the percentage of the dye's contribution to the total system as calculated by Mulliken population analysis. Image adapted with permission ref. [292] Copyright 2016 Royal Society of Chemistry.

With the objective of evaluating the impact of the inclusion MgI_2 additives in the electrolyte composition, that allowed to reach record efficiencies in Fe-NHC DSSCs,[25] we followed the same computational approach used by some of us to model the effect of Li^+ cations at the indoline D102@TiO_2 interfaces,[304] consisting of the addition of a Mg^{2+} cation lying on the top of the TiO_2 surface.[26] The comparison of the PDOS among the molecular backbone and the semiconductor corresponding to the dye-Mg@TiO_2 and dye@TiO_2 surfaces for the homoleptic C1 and heteroleptic ARM13 complexes is presented in Figure 12. Notably, the Mg^{2+} cation strongly interacts with the dye's anchoring group, lying very close to oxygen atoms of the carboxylic moiety (~2.3Å). Therefore, one may expect a more pronounced impact of the cation in those molecular levels localized on the anchoring NHC ligands. The main effect prompted by the presence of the cation in the PDOS features of the pristine surfaces is a negative energy shift which is especially prominent for the unoccupied orbitals of both dyes. In the case of C1, the pristine surface PDOS presents the same characteristics as the ones described above[292] in terms of the nature of the non-/strongly-coupled LUMO/LUMO+1 levels. Nonetheless, since the unoccupied orbitals localized on the anchoring ligand are more affected by the electrostatic effect of the cation, this level becomes the LUMO when Mg^{2+} is adsorbed at the interface, thus contributing to the desired reversal of the interfacial charge separation direction. Regarding ARM13, the incorporation of the cation induces a shift of its LUMO levels, thus falling in the same energy region as the stabilized TiO_2 CB edge. Since the CB edge possess lower density of states, one may expect that the injection rates will decrease upon the shift prompted by the cation. Nonetheless, the larger coupling magnitudes between the LUMO and the CB edge states lead to an increase of about 20% in the injection rates with respect to the values

reported with the pristine TiO_2 surfaces, both for ARM13 and C1.[26] Similar stabilization effects induced by the presence of lithium (Li^+) and tetrabutylammonium (TBA^+) additives in the electrolyte composition were found in $[Fe(bpy\text{-}dca)_2(CNS)_2]^{2+}$ complex dye sensitized based interfaces.[231] Overall, it has been demonstrated the change of the nature of the dye LUMO in C1, the decrease in the injection driving forces, and the largest injection rates, derived from a more efficient coupling with the CB edge, were at the origin of the enhancement of the device performances.[26]

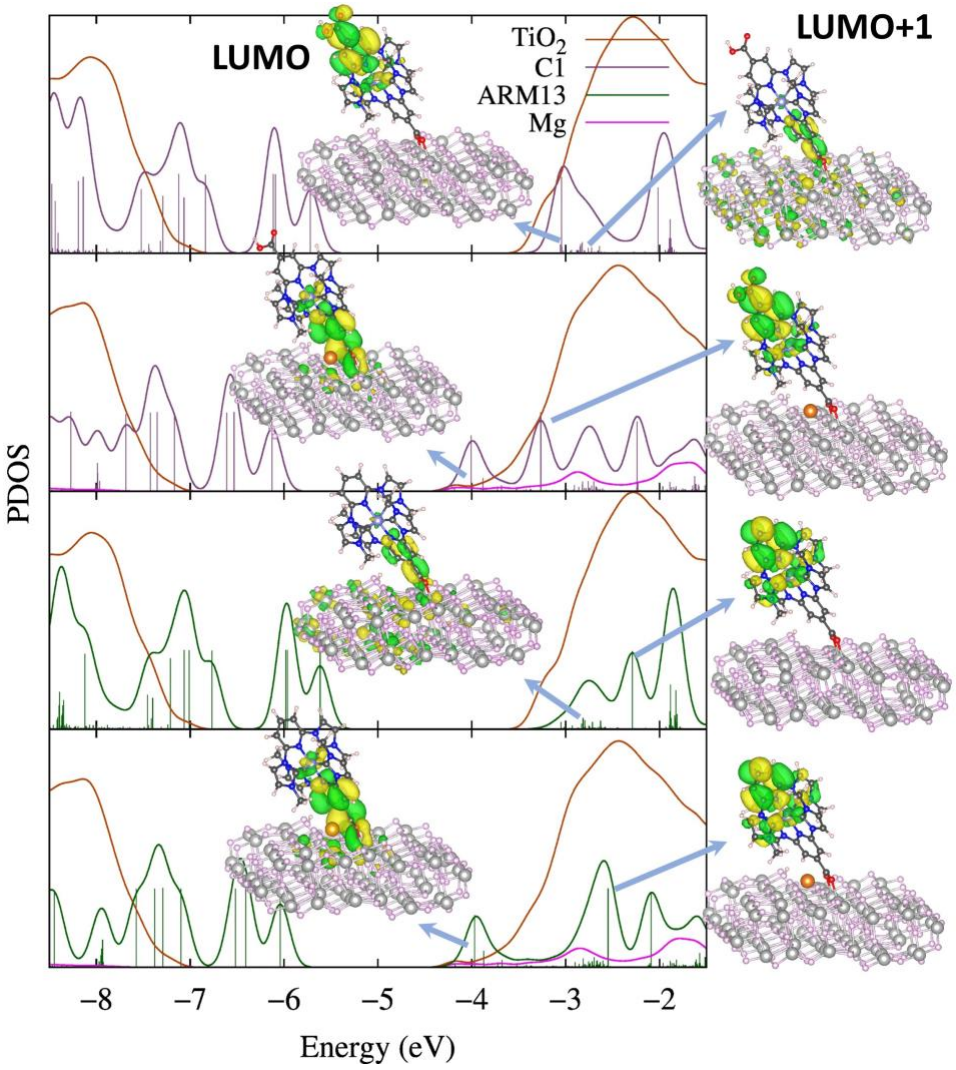

Figure 12. Normalized PDOS over the dye (purple/green for C1/ARM13), TiO_2 surface (orange) and Mg^{2+} cation (magenta) for the C1@TiO_2, C1@Mg-TiO_2, ARM13@TiO_2 and ARM13@Mg-TiO_2 (from the top to the bottom) systems, as obtained from Mulliken population analysis. Vertical bars are used to represent the dye's states conforming the PDOS. The isodensity plots (isovalue 0.02 a.u.) displayed in the onsets of the PDOS plots correspond to the two lowest unoccupied MOs of the dye. Image adapted with permission from ref. [26] Copyright 2021 Royal Society of Chemistry.

Recently, we tackled the modelling of the ARM130-based DSSCs, for which record power conversion efficiencies were recorded. We investigated the electronic structure and charge generation properties of the ARM130@TiO_2 interface, comparing these results with the ones from the unsubstituted dye ARM13.[27] The similar anchoring geometries, injection and recombination rates with respect to the reference ARM13@TiO_2 system, demonstrated that donor substitution is not significantly affecting the interfacial charge generation processes. As a result, the higher efficiencies achieved with ARM130 can be only ascribed to the enhancement of the light harvesting of the MLCT band, as it is showed in Figure 9 left.[27]

6. Conclusions

In this chapter we have presented an extensive overview of the recent advances achieved in modelling DSSCs devices, taking as reference two of the most representative and relevant TMC dye sensitizers used in these technologies, due to their rich photophysics:

the Ru(II) and Fe(II) complexes. After providing a small review of the device operation and the main components integrating the cells, we have focused our discussion on the state-of-start theoretical tools used nowadays to model these components and their interfaces, emphasizing the current challenges and limitations, and finishing by illustrating the main trends in the field aimed to couple these models with experimental data and artificial intelligence in order to carry out a data-driven device design. In a subsequent step, we have evidenced how these methodologies can be applied to tackle the main strategies to optimize TMCs dye sensitizers based cells: (i) the red-shift and intensification of the lowest energy absorption for Ru(II) dyes via enhancement of the SOC effects; (ii) extension of the MLCT lifetimes in Fe(II) complexes by investigation of their minimum energy relaxation paths; and (iii) improvement of the CT occurring at the Fe(II) dye@TiO_2 interface by analyzing the underlying injection/recombination processes and the nature of the dye MLCT bands. These examples clearly evidenced the active role played by the computational chemistry community in the last progress reached in the DSSCs field and corroborated the idea that the development of accurate and still affordable methods to treat complex systems (i.e. solvent/electrolyte environments) and phenomena (i.e. interfacial ET processes or ISCs of the dye states), coupled with experimental measurements dedicated to the fundamental understanding of the physical processes taking place during the device operation, may have a central role in the development of future generation, higher efficient, DSSCs devices.

References

[1] S.N. Singh, P. Tiwari, S. Tiwari, Fundamentals and Innovations in Solar Energy, Springer, 2021. https://doi.org/10.1007/978-981-33-6456-1.

[2] T. Ahmad, D. Zhang, A critical review of comparative global historical energy consumption and future demand: The story told so far, Energy Reports. 6 (2020) 1973–1991. https://doi.org/10.1016/j.egyr.2020.07.020.

[3] S. Sreejith, J. Ajayan, S. Kollem, B. Sivasankari, A Comprehensive Review on Thin Film Amorphous Silicon Solar Cells, Silicon. (2022). https://doi.org/10.1007/s12633-021-01644-w.

[4] J. Yan, B.R. Saunders, Third-generation solar cells: A review and comparison of polymer:fullerene, hybrid polymer and perovskite solar cells, RSC Adv. 4 (2014) 43286–43314. https://doi.org/10.1039/c4ra07064j.

[5] P.K. Nayak, S. Mahesh, H.J. Snaith, D. Cahen, Photovoltaic solar cell technologies: analysing the state of the art, Nat. Rev. Mater. 4 (2019) 269–285. https://doi.org/10.1038/s41578-019-0097-0.

[6] A.B. Muñoz-García, I. Benesperi, G. Boschloo, J.J. Concepcion, J.H. Delcamp, E.A. Gibson, G.J. Meyer, M. Pavone, H. Pettersson, A. Hagfeldt, M. Freitag, Dye-sensitized solar cells strike back, Chem. Soc. Rev. 50 (2021) 12450–12550. https://doi.org/10.1039/d0cs01336f.

[7] M. Kokkonen, P. Talebi, J. Zhou, S. Asgari, S.A. Soomro, F. Elsehrawy, J. Halme, S. Ahmad, A. Hagfeldt, S.G. Hashmi, Advanced research trends in dye-sensitized solar cells, J. Mater. Chem. A. 9 (2021) 10527–10545. https://doi.org/10.1039/d1ta00690h.

[8] H. Gerischer, M.E. Michel-Beyerle, F. Rebentrost, H. Tributsch, Sensitization of charge injection into semiconductors with large band gap, Electrochim. Acta. 13 (1968) 1509–1515. https://doi.org/10.1016/0013-4686(68)80076-3.

[9] O. Brian, M. Grätzel, A low-cost, high-efficiency solar cell based on dye-sensitized colloidal TiO2 films, Nature. 354 (1991) 737–740.

[10] K. Sharma, V. Sharma, S.S. Sharma, Dye-Sensitized Solar Cells: Fundamentals and Current Status, Nanoscale Res. Lett. 13 (2018). https://doi.org/10.1186/s11671-018-2760-6.

[11] A. Hagfeldt, G. Boschloo, L. Sun, L. Kloo, H. Pettersson, Dye-Sensitized Solar Cells, Chem. Rev. 110 (2010) 6595–6663.

[12] M. Grätzel, Dye-sensitized solar cells, J. Photochem. Photobiol. C Photochem. Rev. 4 (2003) 145–153. https://doi.org/10.1016/S1389-5567(03)00026-1.

[13] K. Kakiage, Y. Aoyama, T. Yano, K. Oya, J.I. Fujisawa, M. Hanaya, Highly-efficient dye-sensitized solar cells with collaborative sensitization by silyl-anchor and carboxy-anchor dyes, Chem. Commun. 51 (2015) 15894–15897. https://doi.org/10.1039/c5cc06759f.

[14] Y. Cao, Y. Liu, S.M. Zakeeruddin, A. Hagfeldt, M. Grätzel, Direct Contact of Selective Charge Extraction Layers Enables High-Efficiency Molecular Photovoltaics, Joule. 2 (2018) 1108–1117. https://doi.org/10.1016/j.joule.2018.03.017.

[15] L. Zhang, X. Yang, W. Wang, G.G. Gurzadyan, J. Li, X. Li, J. An, Z. Yu, H. Wang, B. Cai, A. Hagfeldt, L. Sun, 13.6% Efficient organic dye-sensitized solar cells by minimizing energy losses of the excited state, ACS Energy Lett. 4 (2019) 943–951. https://doi.org/10.1021/acsenergylett.9b00141.

[16] D. Zhang, M. Stojanovic, Y. Ren, Y. Cao, F.T. Eickemeyer, E. Socie, N. Vlachopoulos, J.E. Moser, S.M. Zakeeruddin, A. Hagfeldt, M. Grätzel, A

molecular photosensitizer achieves a V oc of 1.24 V enabling highly efficient and stable dye-sensitized solar cells with copper(II/I)-based electrolyte, Nat. Commun. 12 (2021) 2–11. https://doi.org/10.1038/s41467-021-21945-3.

[17] A. Yella, C.L. Mai, S.M. Zakeeruddin, S.N. Chang, C.H. Hsieh, C.Y. Yeh, M. Grätzel, Molecular engineering of push-pull porphyrin dyes for highly efficient dye-sensitized solar cells: The role of benzene spacers, Angew. Chemie - Int. Ed. 53 (2014) 2973–2977. https://doi.org/10.1002/anie.201309343.

[18] S. Mathew, A. Yella, P. Gao, R. Humphry-Baker, B.F.E. Curchod, N. Ashari-Astani, I. Tavernelli, U. Rothlisberger, M.K. Nazeeruddin, M. Grätzel, Dye-sensitized solar cells with 13% efficiency achieved through the molecular engineering of porphyrin sensitizers, Nat. Chem. 6 (2014) 242–247. https://doi.org/10.1038/nchem.1861.

[19] A. Yella, S. Mathew, S. Aghazada, P. Comte, M. Grätzel, M.K. Nazeeruddin, Dye-sensitized solar cells using cobalt electrolytes: the influence of porosity and pore size to achieve high-efficiency, J. Mater. Chem. C. 5 (2017) 2833–2843. https://doi.org/10.1039/c6tc05640g.

[20] C.-P. Lee, R.Y.-Y. Lin, L.-Y. Lin, C.-T. Li, T.-C. Chu, S.-S. Sun, J.T. Linb, K.-C. Ho, Recent progress in organic sensitizers for dye-sensitized solar cells, RSC Adv. 3 (2015) 6053–6063. https://doi.org/10.1039/b000000x.

[21] C.Y. Chen, M. Wang, J.Y. Li, N. Pootrakulchote, L. Alibabaei, C.H. Ngoc-Le, J.D. Decoppet, J.H. Tsai, C. Grätzel, C.G. Wu, S.M. Zakeeruddin, M. Grätzel, Highly efficient light-harvesting ruthenium sensitizer for thin-film dye-sensitized solar cells, ACS Nano. 3 (2009) 3103–3109. https://doi.org/10.1021/nn900756s.

[22] Q. Yu, Y. Wang, Z. Yi, N. Zu, J. Zhang, M. Zhang, P. Wang, High-efficiency dye-sensitized solar cells: The influence of lithium ions on exciton dissociation, charge recombination, and surface states, ACS Nano. 4 (2010) 6032–6038. https://doi.org/10.1021/nn101384e.

[23] F. Sauvage, J.D. Decoppet, M. Zhang, S.M. Zakeeruddin, P. Comte, M. Nazeeruddin, P. Wang, M. Grätzel, Effect of sensitizer adsorption temperature on the performance of dye-sensitized solar cells, J. Am. Chem. Soc. 133 (2011) 9304–9310. https://doi.org/10.1021/ja110541t.

[24] C.C.P. Chiang, C.Y. Hung, S.W. Chou, J.J. Shyue, K.Y. Cheng, P.J. Chang, Y.Y. Yang, C.Y. Lin, T.K. Chang, Y. Chi, H.L. Chou, P.T. Chou, PtCoFe Nanowire Cathodes Boost Short-Circuit Currents of Ru(II)-Based Dye-Sensitized Solar Cells to a Power Conversion Efficiency of 12.29%, Adv. Funct. Mater. 28 (2018) 1–9. https://doi.org/10.1002/adfm.201703282.

[25] E. Marchini, M. Darari, L. Lazzarin, R. Boaretto, R. Argazzi, C.A. Bignozzi, P.C. Gros, S. Caramori, Recombination and regeneration dynamics in FeNHC(ii)-sensitized solar cells, Chem. Commun. 56 (2020) 543–546. https://doi.org/10.1039/c9cc07794d.

[26] A. Reddy-Marri, E. Marchini, V. Diez-Cabanes, R. Argazzi, M. Pastore, S. Caramori, P.C. Gros, Record power conversion efficiencies for Iron (II)-NHC-sensitized DSSCs from rational molecular engineering and electrolyte optimization, J. Mater. Chem. A. 9 (2021) 3540–3554. https://doi.org/doi.org/10.1039/D0TA10841C.

[27] A. Reddy-Marri, E. Marchini, V. Diez-Cabanes, R. Argazzi, M. Pastore, S.

Caramori, C.A. Bignozzi, P.C. Gros, A Series of Iron(II)-NHC Sensitizers with Remarkable Power Conversion Efficiency in Photoelectrochemical Cells, Chem. - A Eur. J. 27 (2021) 16260–16269. https://doi.org/10.1002/chem.202103178.

[28] L. Lindh, O. Gordivska, S. Persson, H. Michaels, H. Fan, P. Chábera, N.W. Rosemann, A.K. Gupta, I. Benesperi, J. Uhlig, O. Prakash, E. Sheibani, K.S. Kjaer, G. Boschloo, A. Yartsev, M. Freitag, R. Lomoth, P. Persson, K. Wärnmark, Dye-sensitized solar cells based on Fe N-heterocyclic carbene photosensitizers with improved rod-like push-pull functionality, Chem. Sci. 12 (2021) 16035–16053.

[29] S. Alhorani, S. Kumar, M. Genwa, P.L. Meena, Review of latest efficient sensitizer in dye-sensitized solar cells, AIP Conf. Proc. 2265 (2020) 5–9. https://doi.org/10.1063/5.0017041.

[30] H. Michaels, M. Rinderle, R. Freitag, I. Benesperi, T. Edvinsson, R. Socher, A. Gagliardi, M. Freitag, Dye-sensitized solar cells under ambient light powering machine learning: Towards autonomous smart sensors for the internet of things, Chem. Sci. 11 (2020) 2895–2906. https://doi.org/10.1039/c9sc06145b.

[31] M. Ye, X. Wen, M. Wang, J. Iocozzia, N. Zhang, C. Lin, Z. Lin, Recent advances in dye-sensitized solar cells: From photoanodes, sensitizers and electrolytes to counter electrodes, Mater. Today. 18 (2015) 155–162. https://doi.org/10.1016/j.mattod.2014.09.001.

[32] K. Fan, J. Yu, W. Ho, Improving photoanodes to obtain highly efficient dye-sensitized solar cells: A brief review, Mater. Horizons. 4 (2017) 319–344. https://doi.org/10.1039/c6mh00511j.

[33] M.E. Yeoh, K.Y. Chan, Recent advances in photo-anode for dye-sensitized solar cells: a review, Int. J. Energy Res. 41 (2017) 2446–2467. https://doi.org/10.1002/er.3764.

[34] X. Liu, J. Fang, Y. Liu, T. Lin, Progress in nanostructured photoanodes for dye-sensitized solar cells, Front. Mater. Sci. 10 (2016) 225–237. https://doi.org/10.1007/s11706-016-0341-0.

[35] M.D. Tyona, R.U. Osuji, F.I. Ezema, A review of zinc oxide photoanode films for dye-sensitized solar cells based on zinc oxide nanostructures, Adv. Nano Res. 1 (2013) 43–58. https://doi.org/10.12989/anr.2013.1.1.043.

[36] R. Vittal, K.C. Ho, Zinc oxide based dye-sensitized solar cells: A review, Renew. Sustain. Energy Rev. 70 (2017) 920–935. https://doi.org/10.1016/j.rser.2016.11.273.

[37] Z. Li, Y. Zhou, R. Sun, Y. Xiong, H. Xie, Z. Zou, Nanostructured SnO2 photoanode-based dye-sensitized solar cells, Chinese Sci. Bull. 59 (2014) 2122–2134. https://doi.org/10.1007/s11434-013-0079-3.

[38] Q. Wali, A. Fakharuddin, R. Jose, Tin oxide as a photoanode for dye-sensitised solar cells: Current progress and future challenges, J. Power Sources. 293 (2015) 1039–1052. https://doi.org/10.1016/j.jpowsour.2015.06.037.

[39] N. Memarian, I. Concina, A. Braga, S.M. Rozati, A. Vomiero, G. Sberveglieri, Hierarchically Assembled ZnO Nanocrystallites for High-Efficiency Dye-Sensitized Solar Cells, Angew. Chemie. 123 (2011) 12529–12533. https://doi.org/10.1002/ange.201104605.

[40] Y.F. Wang, K.N. Li, W.Q. Wu, Y.F. Xu, H.Y. Chen, C.Y. Su, D. Bin Kuang,

Fabrication of a double layered photoanode consisting of SnO2 nanofibers and nanoparticles for efficient dye-sensitized solar cells, RSC Adv. 3 (2013) 13804–13810. https://doi.org/10.1039/c3ra41839a.

[41] E. Benazzi, J. Mallows, G.H. Summers, F.A. Black, E.A. Gibson, Developing photocathode materials for p-type dye-sensitized solar cells, J. Mater. Chem. C. 7 (2019) 10409–10445. https://doi.org/10.1039/c9tc01822k.

[42] J. He, H. Lindström, A. Hagfeldt, S.E. Lindquist, Dye-Sensitized Nanostructured p-Type Nickel Oxide Film as a Photocathode for a Solar Cell, J. Phys. Chem. B. 103 (1999) 8940–8943. https://doi.org/10.1021/jp991681r.

[43] J. He, H. Lindström, A. Hagfeldt, S.E. Lindquist, Dye-sensitized nanostructured tandem cell-first demonstrated cell with a dye-sensitized photocathode, Sol. Energy Mater. Sol. Cells. 62 (2000) 265–273. https://doi.org/10.1016/S0927-0248(99)00168-3.

[44] Y. Farré, M. Raissi, A. Fihey, Y. Pellegrin, E. Blart, D. Jacquemin, F. Odobel, A Blue Diketopyrrolopyrrole Sensitizer with High Efficiency in Nickel-Oxide-based Dye-Sensitized Solar Cells, ChemSusChem. 10 (2017) 2618–2625. https://doi.org/10.1002/cssc.201700468.

[45] H. Iftikhar, G.G. Sonai, S.G. Hashmi, A.F. Nogueira, P.D. Lund, Progress on electrolytes development in dye-sensitized solar cells, 2019. https://doi.org/10.3390/ma12121998.

[46] J. Wu, Z. Lan, J. Lin, M. Huang, Y. Huang, L. Fan, G. Luo, Electrolytes in dye-sensitized solar cells, Chem. Rev. 115 (2015) 2136–2173. https://doi.org/10.1021/cr400675m.

[47] R.A.A. Talip, W.Z.N. Yahya, M.A. Bustam, Ionic liquids roles and perspectives in electrolyte for dye-sensitized solar cells, Sustainability. 12 (2020). https://doi.org/10.3390/su12187598.

[48] Z. Yu, N. Vlachopoulos, M. Gorlov, L. Kloo, Liquid electrolytes for dye-sensitized solar cells, Dalt. Trans. 40 (2011) 10289–10303. https://doi.org/10.1039/c1dt11184a.

[49] B. Li, L. Wang, B. Kang, P. Wang, Y. Qiu, Review of recent progress in solid-state dye-sensitized solar cells, Sol. Energy Mater. Sol. Cells. 90 (2006) 549–573. https://doi.org/10.1016/j.solmat.2005.04.039.

[50] I. Benesperi, H. Michaels, M. Freitag, The researcher's guide to solid-state dye-sensitized solar cells, J. Mater. Chem. C. 6 (2018) 11903–11942. https://doi.org/10.1039/c8tc03542c.

[51] S. Thomas, T.G. Deepak, G.S. Anjusree, T.A. Arun, S. V. Nair, A.S. Nair, A review on counter electrode materials in dye-sensitized solar cells, J. Mater. Chem. A. 2 (2014) 4474–4490. https://doi.org/10.1039/c3ta13374e.

[52] J. Wu, Z. Lan, J. Lin, M. Huang, Y. Huang, L. Fan, G. Luo, Y. Lin, Y. Xie, Y. Wei, Counter electrodes in dye-sensitized solar cells, Chem. Soc. Rev. 46 (2017) 5975–6023. https://doi.org/10.1039/c6cs00752j.

[53] J. Theerthagiri, A.R. Senthil, J. Madhavan, T. Maiyalagan, Recent Progress in Non-Platinum Counter Electrode Materials for Dye-Sensitized Solar Cells, ChemElectroChem. 2 (2015) 928–945. https://doi.org/10.1002/celc.201402406.

[54] X. Wang, B. Zhao, W. Kan, Y. Xie, K. Pan, Review on Low-Cost Counter Electrode Materials for Dye-Sensitized Solar Cells: Effective Strategy to Improve

Photovoltaic Performance, Adv. Mater. Interfaces. 9 (2022) 2101229.

[55] J.N. Clifford, E. Martínez-Ferrero, A. Viterisi, E. Palomares, Sensitizer molecular structure-device efficiency relationship in dye sensitized solar cells, Chem. Soc. Rev. 40 (2011) 1635–1646. https://doi.org/10.1039/b920664g.

[56] S. Shalini, R. Balasundaraprabhu, T.S. Kumar, N. Prabavathy, S. Senthilarasu, S. Prasanna, Status and outlook of sensitizers/dyes used in dye sensitized solar cells (DSSC): a review, Int. J. Energy Res. 40 (2016) 1303–1320. https://doi.org/10.1002/er.3538.

[57] A. Carella, F. Borbone, R. Centore, Research progress on photosensitizers for DSSC, Front. Chem. 6 (2018) 1–24. https://doi.org/10.3389/fchem.2018.00481.

[58] F. Bureš, Fundamental aspects of property tuning in push-pull molecules, RSC Adv. 4 (2014) 58826–58851. https://doi.org/10.1039/c4ra11264d.

[59] A. Mishra, M.K.R. Fischer, P. Büuerle, Metal-Free organic dyes for dye-Sensitized solar cells: From structure: Property relationships to design rules, Angew. Chemie - Int. Ed. 48 (2009) 2474–2499. https://doi.org/10.1002/anie.200804709.

[60] D. Devadiga, M. Selvakumar, P. Shetty, M. Sridhar Santosh, R.S. Chandrabose, S. Karazhanov, Recent developments in metal-free organic sensitizers derived from carbazole, triphenylamine, and phenothiazine for dye-sensitized solar cells, Int. J. Energy Res. 45 (2021) 6584–6643. https://doi.org/10.1002/er.6348.

[61] Ö. Birel, S. Nadeem, H. Duman, Porphyrin-Based Dye-Sensitized Solar Cells (DSSCs): a Review, J. Fluoresc. 27 (2017) 1075–1085. https://doi.org/10.1007/s10895-017-2041-2.

[62] J. Lu, S. Liu, M. Wang, Push-pull zinc porphyrins as light-harvesters for efficient

dye-sensitized solar cells, Front. Chem. 6 (2018). https://doi.org/10.3389/fchem.2018.00541.

[63] Y. Qin, Q. Peng, Ruthenium sensitizers and their applications in dye-sensitized solar cells, Int. J. Photoenergy. 2012 (2012). https://doi.org/10.1155/2012/291579.

[64] S. Aghazada, M.K. Nazeeruddin, Ruthenium Complexes as Sensitizers in Dye-Sensitized Solar Cells, Inorganics. 6 (2018) 52. https://doi.org/10.3390/inorganics6020052.

[65] N. Tomar, A. Agrawal, V.S. Dhaka, P.K. Surolia, Ruthenium complexes based dye sensitized solar cells: Fundamentals and research trends, Sol. Energy. 207 (2020) 59–76. https://doi.org/10.1016/j.solener.2020.06.060.

[66] C.E. Housecroft, E.C. Constable, Solar energy conversion using first row d-block metal coordination compound sensitizers and redox mediators, Chem. Sci. 13 (2022) 1225–1262. https://doi.org/10.1039/d1sc06828h.

[67] B. Bozic-Weber, E.C. Constable, C.E. Housecroft, Light harvesting with Earth abundant d-block metals: Development of sensitizers in dye-sensitized solar cells (DSCs), Coord. Chem. Rev. 257 (2013) 3089–3106. https://doi.org/10.1016/j.ccr.2013.05.019.

[68] J. Conradie, Polypyridyl copper complexes as dye sensitizer and redox mediator for dye-sensitized solar cells, Electrochem. Commun. 134 (2022) 107182. https://doi.org/10.1016/j.elecom.2021.107182.

[69] C.E. Housecroft, E.C. Constable, The emergence of copper(I)-based dye sensitized solar cells, Chem. Soc. Rev. 44 (2015) 8386–8398. https://doi.org/10.1039/c5cs00215j.

[70] O.S. Wenger, Is Iron the New Ruthenium?, Chem. - A Eur. J. 25 (2019) 6043–6052. https://doi.org/10.1002/chem.201806148.

[71] C. Förster, K. Heinze, Photophysics and photochemistry with Earth-abundant metals-fundamentals and concepts, Chem. Soc. Rev. 49 (2020) 1057–1070. https://doi.org/10.1039/c9cs00573k.

[72] M. Sandroni, L. Favereau, A. Planchat, H. Akdas-Kilig, N. Szuwarski, Y. Pellegrin, E. Blart, H. Le Bozec, M. Boujtita, F. Odobel, Heteroleptic copper(i)-polypyridine complexes as efficient sensitizers for dye sensitized solar cells, J. Mater. Chem. A. 2 (2014) 9944–9947. https://doi.org/10.1039/c4ta01755b.

[73] C. Cebrían, M. Pastore, A. Monari, X. Assfeld, P.C. Gros, S. Haacke, Ultrafast Spectroscopy of Fe(II) Complexes Designed for Solar Energy Conversion: Current Status and Open Questions, ChemPhysChem. (2022). https://doi.org/10.1002/cphc.202100659.

[74] S. Ferrere, B.A. Gregg, Photosensitization of TiO2 by [Fe(II)(2,2'-bipyridine-4,4'-dicarboxylic acid)2(CN)2]: Band selective electron injection from ultra-short-lived excited states, J. Am. Chem. Soc. 120 (1998) 843–844. https://doi.org/10.1021/ja973504e.

[75] S. Ferrere, New Photosensitizers Based upon [Fe(L)2(CN)2] and [Fe(L)3](L) Substituted 2,2′-Bipyridine): Yields for the Photosensitization of TiO2 and Effects on the Band Selectivity, Chem. Mater. 12 (2000) 1083–1089.

[76] J.E. Monat, J.K. McCusker, Femtosecond excited-state dynamics of an iron(II) polypyridyl solar cell sensitizer model, J. Am. Chem. Soc. 122 (2000) 4092–4097. https://doi.org/10.1021/ja992436o.

[77] Y. Liu, P. Persson, V. Sundström, K. Wärnmark, Fe N-Heterocyclic Carbene Complexes as Promising Photosensitizers, Acc. Chem. Res. 49 (2016) 1477–1485. https://doi.org/10.1021/acs.accounts.6b00186.

[78] T. Duchanois, L. Liu, M. Pastore, A. Monari, C. Cebrián, Y. Trolez, M. Darari, K. Magra, A. Francés-Monerris, E. Domenichini, M. Beley, X. Assfeld, S. Haacke, P. Gros, NHC-Based Iron Sensitizers for DSSCs, Inorganics. 6 (2018) 63. https://doi.org/10.3390/inorganics6020063.

[79] T. Duchanois, T. Etienne, C. Cebrián, L. Liu, A. Monari, M. Beley, X. Assfeld, S. Haacke, P.C. Gros, An iron-based photosensitizer with extended excited-state lifetime: Photophysical and photovoltaic properties, Eur. J. Inorg. Chem. 2015 (2015) 2469–2477. https://doi.org/10.1002/ejic.201500142.

[80] T.C.B. Harlang, Y. Liu, O. Gordivska, L.A. Fredin, C.S. Ponseca, P. Huang, P. Chábera, K.S. Kjaer, H. Mateos, J. Uhlig, R. Lomoth, R. Wallenberg, S. Styring, P. Persson, V. Sundström, K. Wärnmark, Iron sensitizer converts light to electrons with 92% yield, Nat. Chem. 7 (2015) 883–889. https://doi.org/10.1038/nchem.2365.

[81] L. Liu, T. Duchanois, T. Etienne, A. Monari, M. Beley, X. Assfeld, S. Haacke, P.C. Gros, A new record excited state 3MLCT lifetime for metalorganic iron(II) complexes, Phys. Chem. Chem. Phys. 18 (2016) 12550–12556. https://doi.org/10.1039/c6cp01418f.

[82] S. Kaufhold, K. Wärnmark, Design and synthesis of photoactive iron n-heterocyclic carbene complexes, Catalysts. 10 (2020) 132. https://doi.org/10.3390/catal10010132.

[83] L. Lindh, P. Chábera, N.W. Rosemann, J. Uhlig, K. Wärnmark, A. Yartsev, V. Sundström, P. Persson, Photophysics and photochemistry of iron carbene complexes for solar energy conversion and photocatalysis, Catalysts. 10 (2020) 315. https://doi.org/10.3390/catal10030315.

[84] M. Darari, E. Domenichini, A. Francés-Monerris, C. Cebrián, K. Magra, M. Beley, M. Pastore, A. Monari, X. Assfeld, S. Haacke, P.C. Gros, Iron(ii) complexes with diazinyl-NHC ligands: Impact of π-deficiency of the azine core on photophysical properties, Dalt. Trans. 48 (2019) 10915–10926. https://doi.org/10.1039/c9dt01731c.

[85] J.D. Braun, I.B. Lozada, C. Kolodziej, C. Burda, K.M.E. Newman, J. van Lierop, R.L. Davis, D.E. Herbert, Iron(ii) coordination complexes with panchromatic absorption and nanosecond charge-transfer excited state lifetimes, Nat. Chem. 11 (2019) 1144–1150. https://doi.org/10.1038/s41557-019-0357-z.

[86] F. Labat, I. Ciofini, H.P. Hratchian, M.J. Frisch, K. Raghavachari, C. Adamo, Insights into working principles of ruthenium polypyridyl dye-sensitized solar cells from first principles modeling, J. Phys. Chem. C. 115 (2011) 4297–4306. https://doi.org/10.1021/jp108917c.

[87] F. Labat, T. Le Bahers, I. Ciofini, C. Adamo, First-principles modeling of dye-sensitized solar cells: Challenges and perspectives, Acc. Chem. Res. 45 (2012) 1268–1277. https://doi.org/10.1021/ar200327w.

[88] M. Pastore, S. Fantacci, F. De Angelis, Modeling excited states and alignment of energy levels in dye-sensitized solar cells: Successes, failures, and challenges, J. Phys. Chem. C. 117 (2013) 3685–3700. https://doi.org/10.1021/jp3095227.

[89] T. Le Bahers, T. Pauporté, P.P. Lainé, F. Labat, C. Adamo, I. Ciofini, Modeling dye-sensitized solar cells: From theory to experiment, J. Phys. Chem. Lett. 4 (2013) 1044–1050. https://doi.org/10.1021/jz400046p.

[90] M. Pastore, A. Selloni, S. Fantacci, F. De Angelis, Electronic and Optical Properties of Dye-Sensitized TiO2 Interfaces, Top Curr Chem. (2014) 1–45. https://doi.org/10.1007/128_2013_507.

[91] M. Pastore, First principle modelling of materials and processes in dye-sensitized photoanodes for solar energy and solar fuels, Computation. 5 (2017). https://doi.org/10.3390/computation5010005.

[92] T. Le Bahers, F. Labat, T. Pauporté, P.P. Lainé, I. Ciofini, Theoretical procedure for optimizing dye-sensitized solar cells: From electronic structure to photovoltaic efficiency, J. Am. Chem. Soc. 133 (2011) 8005–8013. https://doi.org/10.1021/ja201944g.

[93] O.S. Al-Qurashi, N. Wazzan, Prediction of Power Conversion Efficiencies of Diphenylthienylamine-Based Dyes Adsorbed on the Titanium Dioxide Nanotube, ACS Omega. 6 (2021) 8967–8975. https://doi.org/10.1021/acsomega.0c06340.

[94] M. Pastore, T. Etienne, F. De Angelis, Structural and electronic properties of dye-sensitized TiO2 for solar cell applications: From single molecules to self-assembled monolayers, J. Mater. Chem. C. 4 (2016) 4346–4373. https://doi.org/10.1039/c6tc00554c.

[95] F. De Angelis, C. Di Valentin, S. Fantacci, A. Vittadini, A. Selloni, Theoretical studies on anatase and less common TiO2 phases: Bulk, surfaces, and nanomaterials, Chem. Rev. 114 (2014) 9708–9753.

https://doi.org/10.1021/cr500055q.

[96] M.J. Lundqvist, M. Nilsing, P. Persson, S. Lunell, DFT Study of Bare and Dye-Sensitized TiO2 Clusters and Nanocrystals, Int. J. Quantum Chem. 106 (2006) 3214–3234. https://doi.org/10.1002/qua.21088.

[97] F. Nunzi, E. Mosconi, L. Storchi, E. Ronca, A. Selloni, M. Grätzel, F. De Angelis, Inherent electronic trap states in TiO2 nanocrystals: Effect of saturation and sintering, Energy Environ. Sci. 6 (2013) 1221–1229. https://doi.org/10.1039/c3ee24100a.

[98] H. Watanabe, K. Fujikata, Y. Oaki, H. Imai, Band-gap expansion of tungsten oxide quantum dots synthesized in sub-nano porous silica, Chem. Commun. 49 (2013) 8477–8479. https://doi.org/10.1039/c3cc44264k.

[99] M.L. Kahn, T. Cardinal, B. Bousquet, M. Monge, V. Jubera, B. Chaudret, Optical properties of zinc oxide nanoparticles and nanorods synthesized using an organometallic method, ChemPhysChem. 7 (2006) 2392–2397. https://doi.org/10.1002/cphc.200600184.

[100] V. Diez-Cabanes, A. Morales-Garcia, F. Illas, M. Pastore, Understanding the Structural and Electronic Properties of Photoactive Tungsten Oxide Nanoparticles from Density Functional Theory and GW Approaches, J. Chem. Theory Comput. 17 (2021) 3462–3470. https://doi.org/doi.org/10.1021/acs.jctc.1c00293.

[101] E. Galoppini, Linkers for anchoring sensitizers to semiconductor nanoparticles, Coord. Chem. Rev. 248 (2004) 1283–1297. https://doi.org/10.1016/j.ccr.2004.03.016.

[102] M. Pastore, F. De Angelis, Computational modelling of TiO2 surfaces sensitized

by organic dyes with different anchoring groups: Adsorption modes, electronic structure and implication for electron injection/recombination, Phys. Chem. Chem. Phys. 14 (2012) 920–928. https://doi.org/10.1039/c1cp22663k.

[103] L. Zhang, J.M. Cole, Anchoring groups for dye-sensitized solar cells, ACS Appl. Mater. Interfaces. 7 (2015) 3427–3455. https://doi.org/10.1021/am507334m.

[104] F. Ambrosio, N. Martsinovich, A. Troisi, What is the best anchoring group for a dye in a dye-sensitized solar cell?, J. Phys. Chem. Lett. 3 (2012) 1531–1535. https://doi.org/10.1021/jz300520p.

[105] I. Arbouch, D. Cornil, Y. Karzazi, B. Hammouti, R. Lazzaroni, J. Cornil, Influence of the nature of the anchoring group on electron injection processes at dye-titania interfaces, Phys. Chem. Chem. Phys. 19 (2017) 29389–29401. https://doi.org/10.1039/c7cp05638a.

[106] A. Ben Jannet, M. Said, M. Badawi, M. Pastore, First-Principles Modeling of Dye Anchoring on (001) γ-Monoclinic WO 3 Surfaces: The Role of Oxygen Vacancies, J. Phys. Chem. C. 126 (2022) 5424–5434. https://doi.org/10.1021/acs.jpcc.1c10397.

[107] D. Dimple, S. Lebègue, M. Pastore, Dye Anchoring on CuCrO2Surfaces for p-Type Dye-Sensitized Solar Cell Applications: An Ab Initio Study, ACS Appl. Energy Mater. 4 (2021) 6180–6190. https://doi.org/10.1021/acsaem.1c00970.

[108] S. Piccinin, D. Rocca, M. Pastore, Role of Solvent in the Energy Level Alignment of Dye-Sensitized NiO Interfaces, J. Phys. Chem. C. 121 (2017) 22286–22294. https://doi.org/10.1021/acs.jpcc.7b08463.

[109] E. Bae, W. Choi, J. Park, H.S. Shin, S. Bin Kim, J.S. Lee, Effects of Surface

Anchoring Groups (Carboxylate vs Phosphonate) in Ruthenium-Complex-Sensitized TiO2 on Visible Light Reactivity in Aqueous Suspensions, J. Phys. Chem. B. 108 (2004) 14093–14101.

[110] X. Zhang, T. Peng, S. Song, Recent advances in dye-sensitized semiconductor systems for photocatalytic hydrogen production, J. Mater. Chem. A. 4 (2016) 2365–2402. https://doi.org/10.1039/c5ta08939e.

[111] P. Pechy, F.P. Rotzinger, M.K. Nazeeruddin, O. Kohle, S.M. Zakeeruddin, R. Humphry-baker, M. Gratzel, Preparation of Phosphonated Polypyridyl Ligands to anchor Transition-metal Complexes on Oxide Surfaces: Application for the Conversion of Light to Electricity with Nanocrystalline TO2 Films Peter, J. Chem. Soc., Chem. Commun. (1995) 65–66.

[112] S. Akin, S. Açikgöz, M. Gülen, C. Akyürek, S. Sönmezoğlu, Investigation of the photoinduced electron injection processes for natural dye-sensitized solar cells: The impact of anchoring groups, RSC Adv. 6 (2016) 85125–85134. https://doi.org/10.1039/c6ra19653e.

[113] T.T. Li, B. Shan, T.J. Meyer, Stable Molecular Photocathode for Solar-Driven CO 2 Reduction in Aqueous Solutions, ACS Energy Lett. 4 (2019) 629–636. https://doi.org/10.1021/acsenergylett.8b02512.

[114] K.L. Materna, J. Jiang, R.H. Crabtree, G.W. Brudvig, Silatrane Anchors for Metal Oxide Surfaces: Optimization for Potential Photocatalytic and Electrocatalytic Applications, ACS Appl. Mater. Interfaces. 11 (2019) 5602–5609. https://doi.org/10.1021/acsami.8b04138.

[115] W. Li, L.G.C. Rego, F.Q. Bai, J. Wang, R. Jia, L.M. Xie, H.X. Zhang, What makes

hydroxamate a promising anchoring group in dye-sensitized solar cells? Insights from theoretical investigation, J. Phys. Chem. Lett. 5 (2014) 3992–3999. https://doi.org/10.1021/jz501973d.

[116] J. Tomasi, B. Mennucci, R. Cammi, Quantum mechanical continuum solvation models, Chem. Rev. 105 (2005) 2999–3093. https://doi.org/10.1021/cr9904009.

[117] A. Klamt, G. Schüürmann, COSMO: A new approach to dielectric screening in solvents with explicit expressions for the screening energy and its gradient, J. Chem. Soc. Perkin Trans. 2. (1993) 799–805. https://doi.org/10.1039/P29930000799.

[118] A. Segalina, S. Lebègue, D. Rocca, S. Piccinin, M. Pastore, Structure and Energetics of Dye-Sensitized NiO Interfaces in Water from Ab Initio MD and Large-Scale GW Calculations, J. Chem. Theory Comput. 17 (2021) 5225–5238. https://doi.org/10.1021/acs.jctc.1c00354.

[119] Y. Tateyama, M. Sumita, Y. Ootani, K. Aikawa, R. Jono, L. Han, K. Sodeyama, Acetonitrile solution effect on Ru N749 dye adsorption and excitation at TiO2 anatase interface, J. Phys. Chem. C. 118 (2014) 16863–16871. https://doi.org/10.1021/jp5004006.

[120] G. Prampolini, F. Ingrosso, J. Cerezo, A. Iagatti, P. Foggi, M. Pastore, Short- and Long-Range Solvation Effects on the Transient UV-Vis Absorption Spectra of a Ru(II)-Polypyridine Complex Disentangled by Nonequilibrium Molecular Dynamics, J. Phys. Chem. Lett. 10 (2019) 2885–2891. https://doi.org/10.1021/acs.jpclett.9b00944.

[121] G. Prampolini, F. Ingrosso, A. Segalina, S. Caramori, P. Foggi, M. Pastore,

Dynamical and Environmental Effects on the Optical Properties of an Heteroleptic Ru(II)-Polypyridine Complex: A Multilevel Approach Combining Accurate Ground and Excited State QM-Derived Force Fields, MD and TD-DFT, J. Chem. Theory Comput. 15 (2019) 529–545. https://doi.org/10.1021/acs.jctc.8b01031.

[122] V. Diez-Cabanes, G. Prampolini, A. Francés-Monerris, A. Monari, M. Pastore, Iron's Wake: The Performance of Quantum Mechanical-Derived Versus General-Purpose Force Fields Tested on a Luminescent Iron Complex, Molecules. 25 (2020) 3084. https://doi.org/10.3390/molecules25133084.

[123] I. Tavernelli, B.F.E. Curchod, U. Rothlisberger, Nonadiabatic molecular dynamics with solvent effects: A LR-TDDFT QM/MM study of ruthenium (II) tris (bipyridine) in water, Chem. Phys. 391 (2011) 101–109. https://doi.org/10.1016/j.chemphys.2011.03.021.

[124] M.E. Moret, I. Tavernelli, U. Rothlisberger, Combined QM/MM and classical molecular dynamics study of [Ru(bpy) 3]2+ in water, J. Phys. Chem. B. 113 (2009) 7737–7744. https://doi.org/10.1021/jp900147r.

[125] G. Fazio, D. Selli, L. Ferraro, G. Seifert, C. Di Valentin, Curved TiO2 Nanoparticles in Water: Short (Chemical) and Long (Physical) Range Interfacial Effects, ACS Appl. Mater. Interfaces. 10 (2018) 29943–29953. https://doi.org/10.1021/acsami.8b08172.

[126] W. Kohn, Nobel Lecture: Electronic structure of matter—wave functions and density functionals, Rev. Mod. Phys. 71 (1999) 1253–1266. https://doi.org/10.1103/RevModPhys.71.1253.

[127] C. Adamo, D. Jacquemin, The calculations of excited-state properties with time-

dependent density functional theory, Chem. Soc. Rev. 42 (2013) 845–856. https://doi.org/10.1039/c2cs35394f.

[128] A.D. Laurent, C. Adamo, D. Jacquemin, Dye chemistry with time-dependent density functional theory, Phys. Chem. Chem. Phys. 16 (2014) 14334–14356. https://doi.org/10.1039/c3cp55336a.

[129] J.P. Perdew, J.A. Chevary, S.H. Vosko, K.A. Jackson, M.R. Pederson, D.J. Singh, C. Fiolhais, Atoms, molecules, solids, and surfaces: Applications of the generalized gradient approximation for exchange and correlation, Phys. Rev. B. 48 (1993) 4978. https://doi.org/10.1103/PhysRevB.48.4978.2.

[130] J.P. Perdew, K. Burke, M. Ernzerhof, Generalized Gradient Approximation Made Simple, Phys. Rev. Lett. 77 (1996) 3865–3868. https://doi.org/10.1103/PhysRevLett.77.3865.

[131] C. Lee, W. Yang, R.G. Parr, Development of the Colic Salvetti correlation-energy into a functional of the electron density formula Chengteh, Phys. Rev. B. 37 (1988) 785–789.

[132] M.J.G. Peach, P. Benfield, T. Helgaker, D.J. Tozer, Excitation energies in density functional theory: An evaluation and a diagnostic test, J. Chem. Phys. 128 (2008). https://doi.org/10.1063/1.2831900.

[133] P. Dev, S. Agrawal, N.J. English, Determining the appropriate exchange-correlation functional for time-dependent density functional theory studies of charge-transfer excitations in organic dyes, J. Chem. Phys. 136 (2012). https://doi.org/10.1063/1.4725540.

[134] A. Dreuw, J.L. Weisman, M. Head-Gordon, Long-range charge-transfer excited

states in time-dependent density functional theory require non-local exchange, J. Chem. Phys. 119 (2003) 2943–2946. https://doi.org/10.1063/1.1590951.

[135] D.J. Tozer, Relationship between long-range charge-transfer excitation energy error and integer discontinuity in Kohn-Sham theory, J. Chem. Phys. 119 (2003) 12697–12699. https://doi.org/10.1063/1.1633756.

[136] D. Jacquemin, E.A. Perpète, G.E. Scuseria, I. Ciofini, C. Adamo, TD-DFT performance for the visible absorption spectra of organic dyes: Conventional versus long-range hybrids, J. Chem. Theory Comput. 4 (2008) 123–135. https://doi.org/10.1021/ct700187z.

[137] A. Dreuw, M. Head-Gordon, Single-reference ab initio methods for the calculation of excited states of large molecules, Chem. Rev. 105 (2005) 4009–4037. https://doi.org/10.1021/cr0505627.

[138] A. Migani, D.J. Mowbray, J. Zhao, H. Petek, A. Rubio, Quasiparticle level alignment for photocatalytic interfaces, J. Chem. Theory Comput. 10 (2014) 2103–2113. https://doi.org/10.1021/ct500087v.

[139] D. Gemeri, J.C. Tremblay, M. Pastore, H. Bahmann, Electronic structure, optical properties, and electron dynamics in organic dye-sensitized TiO2 interfaces by local hybrid density functionals, Chem. Phys. 559 (2022) 111521. https://doi.org/10.1016/j.chemphys.2022.111521.

[140] W. Chen, G. Miceli, G.M. Rignanese, A. Pasquarello, Nonempirical dielectric-dependent hybrid functional with range separation for semiconductors and insulators, Phys. Rev. Mater. 2 (2018) 1–14. https://doi.org/10.1103/PhysRevMaterials.2.073803.

[141] N.P. Brawand, M. Vörös, M. Govoni, G. Galli, Generalization of dielectric-Dependent hybrid functionals to finite systems, Phys. Rev. X. 6 (2016) 041002. https://doi.org/10.1103/PhysRevX.6.041002.

[142] Mariachiara Pastore, Edoardo Mosconi, Simona Fantacci, Filippo De Angelis, Computational Investigations on Organic Sensitizers for Dye-Sensitized Solar Cell, Curr. Org. Synth. 9 (2012) 215–232. https://doi.org/10.2174/157017912799828987.

[143] H. Iikura, T. Tsuneda, T. Yanai, K. Hirao, A long-range correction scheme for generalized-gradient-approximation exchange functionals, J. Chem. Phys. 115 (2001) 3540–3544. https://doi.org/10.1063/1.1383587.

[144] Y. Tawada, T. Tsuneda, S. Yanagisawa, T. Yanai, K. Hirao, A long-range-corrected time-dependent density functional theory, J. Chem. Phys. 120 (2004) 8425–8433. https://doi.org/10.1063/1.1688752.

[145] M. Kamiya, H. Sekino, T. Tsuneda, K. Hirao, Nonlinear optical property calculations by the long-range-corrected coupled-perturbed Kohn-Sham method, J. Chem. Phys. 122 (2005). https://doi.org/10.1063/1.1935514.

[146] J. Da Chai, M. Head-Gordon, Systematic optimization of long-range corrected hybrid density functionals, J. Chem. Phys. 128 (2008). https://doi.org/10.1063/1.2834918.

[147] T. Yanai, D.P. Tew, N.C. Handy, A new hybrid exchange-correlation functional using the Coulomb-attenuating method (CAM-B3LYP), Chem. Phys. Lett. 393 (2004) 51–57. https://doi.org/10.1016/j.cplett.2004.06.011.

[148] J. Da Chai, M. Head-Gordon, Long-range corrected hybrid density functionals

with damped atom-atom dispersion corrections, Phys. Chem. Chem. Phys. 10 (2008) 6615–6620. https://doi.org/10.1039/b810189b.

[149] J. Jaramillo, G.E. Scuseria, M. Ernzerhof, Local hybrid functionals, J. Chem. Phys. 118 (2003) 1068–1073. https://doi.org/10.1063/1.1528936.

[150] J.P. Perdew, V.N. Staroverov, J. Tao, G.E. Scuseria, Density functional with full exact exchange, balanced nonlocality of correlation, and constraint satisfaction, Phys. Rev. A - At. Mol. Opt. Phys. 78 (2008) 1–13. https://doi.org/10.1103/PhysRevA.78.052513.

[151] H. Bahmann, A. Rodenberg, A. V. Arbuznikov, M. Kaupp, A thermochemically competitive local hybrid functional without gradient corrections, J. Chem. Phys. 126 (2007). https://doi.org/10.1063/1.2429058.

[152] E. Kraisler, T. Schmidt, S. Kümmel, L. Kronik, Effect of ensemble generalization on the highest-occupied Kohn-Sham eigenvalue, J. Chem. Phys. 143 (2015). https://doi.org/10.1063/1.4930119.

[153] P. De Silva, C. Corminboeuf, Local hybrid functionals with orbital-free mixing functions and balanced elimination of self-interaction error, J. Chem. Phys. 142 (2015) 1–13. https://doi.org/10.1063/1.4908148.

[154] T.M. Maier, A. V. Arbuznikov, M. Kaupp, Local hybrid functionals: Theory, implementation, and performance of an emerging new tool in quantum chemistry and beyond, Wiley Interdiscip. Rev. Comput. Mol. Sci. 9 (2019) 1–32. https://doi.org/10.1002/wcms.1378.

[155] P. Møller, MP2 notes, Eur. J. Cardio-Thoracic Surg. 53 (1934) 1237–1243.

[156] R.J. Bartlett, M. Musiał, Coupled-cluster theory in quantum chemistry, Rev. Mod.

Phys. 79 (2007) 291–352. https://doi.org/10.1103/RevModPhys.79.291.

[157] G.P. Chen, V.K. Voora, M.M. Agee, S.G. Balasubramani, F. Furche, Random-Phase Approximation Methods, Annu. Rev. Phys. Chem. 68 (2017) 421–445.

[158] S. Grimme, A. Hansen, J.G. Brandenburg, C. Bannwarth, Dispersion-Corrected Mean-Field Electronic Structure Methods, Chem. Rev. 116 (2016) 5105–5154. https://doi.org/10.1021/acs.chemrev.5b00533.

[159] D. Chakraborty, K. Berland, T. Thonhauser, Next-Generation Nonlocal van der Waals Density Functional, J. Chem. Theory Comput. 16 (2020) 5893–5911. https://doi.org/10.1021/acs.jctc.0c00471.

[160] O.A. Vydrov, T. Van Voorhis, Nonlocal van der Waals density functional: The simpler the better, J. Chem. Phys. 133 (2010). https://doi.org/10.1063/1.3521275.

[161] S. Grimme, J. Antony, S. Ehrlich, H. Krieg, A consistent and accurate ab initio parametrization of density functional dispersion correction (DFT-D) for the 94 elements H-Pu, J. Chem. Phys. 132 (2010). https://doi.org/10.1063/1.3382344.

[162] A. Tkatchenko, M. Scheffler, Accurate molecular van der Waals interactions from ground-state electron density and free-atom reference data, Phys. Rev. Lett. 102 (2009) 6–9. https://doi.org/10.1103/PhysRevLett.102.073005.

[163] A.D. Becke, E.R. Johnson, A density-functional model of the dispersion interaction, J. Chem. Phys. 123 (2005). https://doi.org/10.1063/1.2065267.

[164] R. Peverati, D.G. Truhlar, Quest for a universal density functional: The accuracy of density functionals across a broad spectrum of databases in chemistry and physics, Philos. Trans. R. Soc. A Math. Phys. Eng. Sci. 372 (2014). https://doi.org/10.1098/rsta.2012.0476.

[165] S.M. Dancoff, Non-Adiabatic Meson Theory of Nuclear Forces, Phys. Rev. 78 (1950) 382–385.

[166] M.J.G. Peach, M.J. Williamson, D.J. Tozer, Influence of triplet instabilities in TDDFT, J. Chem. Theory Comput. 7 (2011) 3578–3585. https://doi.org/10.1021/ct200651r.

[167] M. Chergui, Ultrafast Photophysics of Transition Metal Complexes, Acc. Chem. Res. 48 (2015) 801–808. https://doi.org/10.1021/ar500358q.

[168] A. Fouqueau, S. Mer, M.E. Casida, L.M.L. Daku, A. Hauser, T. Mineva, F. Neese, Comparison of density functionals for energy and structural differences between the high- [5T2g: (t2g)4(eg)2] and low- [1A1g:(t2g)6(eg)2] spin states of the hexaquoferrous cation [Fe(H2O)6]2+, J. Chem. Phys. 120 (2004) 9473–9486. https://doi.org/10.1063/1.1710046.

[169] F. Neese, Prediction of molecular properties and molecular spectroscopy with density functional theory: From fundamental theory to exchange-coupling, Coord. Chem. Rev. 253 (2009) 526–563. https://doi.org/10.1016/j.ccr.2008.05.014.

[170] M. Swart, A.R. Groenhof, A.W. Ehlers, K. Lammertsma, Validation of exchange-correlation functional for spin states of iron complexes, J. Phys. Chem. A. 108 (2004) 5479–5483. https://doi.org/10.1021/jp049043i.

[171] M. Reiher, Theoretical study of the Fe(phen)2(NCS)2 spin-crossover complex with reparametrized density functionals, Inorg. Chem. 41 (2002) 6928–6935. https://doi.org/10.1021/ic0258911.

[172] M. Pápai, T.J. Penfold, K.B. Møller, Effect of tert-Butyl Functionalization on the Photoexcited Decay of a Fe(II)-N-Heterocyclic Carbene Complex, J. Phys. Chem.

C. 120 (2016) 17234–17241. https://doi.org/10.1021/acs.jpcc.6b05023.

[173] R.L. Lord, F.A. Schultz, M.H. Baik, Spin crossover-coupled electron transfer of [M(tacn) 2] 3+/2+ complexes (tacn) 1,4,7-triazacyclononane; M = Cr Mn Fe Co Ni), J. Am. Chem. Soc. 131 (2009) 6189–6197. https://doi.org/10.1021/ja809552p.

[174] K.P. Kepp, Theoretical Study of Spin Crossover in 30 Iron Complexes, Inorg. Chem. 55 (2016) 2717–2727. https://doi.org/10.1021/acs.inorgchem.5b02371.

[175] J. Cirera, M. Via-Nadal, E. Ruiz, Benchmarking Density Functional Methods for Calculation of State Energies of First Row Spin-Crossover Molecules, Inorg. Chem. 57 (2018) 14097–14105. https://doi.org/10.1021/acs.inorgchem.8b01821.

[176] G. Prokopiou, L. Kronik, Spin-State Energetics of Fe Complexes from an Optimally Tuned Range-Separated Hybrid Functional, Chem. - A Eur. J. 24 (2018) 5173–5182. https://doi.org/10.1002/chem.201704014.

[177] E.I. Ioannidis, H.J. Kulik, Ligand-field-dependent behavior of meta-GGA exchange in transition-metal complex spin-state ordering, J. Phys. Chem. A. 121 (2017) 874–884. https://doi.org/10.1021/acs.jpca.6b11930.

[178] S. Grimme, Semiempirical hybrid density functional with perturbative second-order correlation, J. Chem. Phys. 124 (2006). https://doi.org/10.1063/1.2148954.

[179] S. Ye, F. Neese, Accurate modeling of spin-state energetics in spin-crossover systems with modern density functional theory, Inorg. Chem. 49 (2010) 772–774. https://doi.org/10.1021/ic902365a.

[180] L. Wilbraham, C. Adamo, I. Ciofini, Communication: Evaluating non-empirical double hybrid functionals for spin-state energetics in transition-metal complexes, J. Chem. Phys. 148 (2018). https://doi.org/10.1063/1.5019641.

[181] B. Himmetoglu, A. Floris, S. De Gironcoli, M. Cococcioni, Hubbard-corrected DFT energy functionals: The LDA+U description of correlated systems, Int. J. Quantum Chem. 114 (2014) 14–49. https://doi.org/10.1002/qua.24521.

[182] L.A. Mariano, B. Vlaisavljevich, R. Poloni, Improved Spin-State Energy Differences of Fe(II) Molecular and Crystalline Complexes via the Hubbard U-Corrected Density, J. Chem. Theory Comput. 17 (2021) 2807–2816. https://doi.org/10.1021/acs.jctc.1c00034.

[183] L. Petit, P. Maldivi, C. Adamo, Predictions of optical excitations in transition-metal complexes with time dependent-Density Functional Theory: Influence of basis sets, J. Chem. Theory Comput. 1 (2005) 953–962. https://doi.org/10.1021/ct0500500.

[184] L. Wilbraham, P. Verma, D.G. Truhlar, L. Gagliardi, I. Ciofini, Multiconfiguration Pair-Density Functional Theory Predicts Spin-State Ordering in Iron Complexes with the Same Accuracy as Complete Active Space Second-Order Perturbation Theory at a Significantly Reduced Computational Cost, J. Phys. Chem. Lett. 8 (2017) 2026–2030. https://doi.org/10.1021/acs.jpclett.7b00570.

[185] A. Domingo, M.À. Carvajal, C. de Graaf, Spin Crossover in Fe(II) Complexes: An Ab Initio Study of Ligand σ-Donation, Int. J. Quantum Chem. 110 (2009) 331–337. https://doi.org/10.1002/qua.22105.

[186] K. Pierloot, Q.M. Phung, A. Domingo, Spin State Energetics in First-Row Transition Metal Complexes: Contribution of (3s3p) Correlation and Its Description by Second-Order Perturbation Theory, J. Chem. Theory Comput. 13 (2017) 537–553. https://doi.org/10.1021/acs.jctc.6b01005.

[187] Q.M. Phung, M. Feldt, J.N. Harvey, K. Pierloot, Toward Highly Accurate Spin State Energetics in First-Row Transition Metal Complexes: A Combined CASPT2/CC Approach, J. Chem. Theory Comput. 14 (2018) 2446–2455. https://doi.org/10.1021/acs.jctc.8b00057.

[188] M. Radoń, Benchmarking quantum chemistry methods for spin-state energetics of iron complexes against quantitative experimental data, Phys. Chem. Chem. Phys. 21 (2019) 4854–4870. https://doi.org/10.1039/c9cp00105k.

[189] F. Neese, T. Petrenko, D. Ganyushin, G. Olbrich, Advanced aspects of ab initio theoretical optical spectroscopy of transition metal complexes: Multiplets, spin-orbit coupling and resonance Raman intensities, Coord. Chem. Rev. 251 (2007) 288–327. https://doi.org/10.1016/j.ccr.2006.05.019.

[190] M. Radoń, Revisiting the role of exact exchange in DFT spin-state energetics of transition metal complexes, Phys. Chem. Chem. Phys. 16 (2014) 14479–14488. https://doi.org/10.1039/c3cp55506b.

[191] E.I. Ioannidis, H.J. Kulik, Towards quantifying the role of exact exchange in predictions of transition metal complex properties, J. Chem. Phys. 143 (2015). https://doi.org/10.1063/1.4926836.

[192] C. Chang, M. Pelissier, P. Durand, Regular two-component pauli-like effective hamiltonians in dirac theory, Phys. Scr. 34 (1986) 394–404. https://doi.org/10.1088/0031-8949/34/5/007.

[193] E. Van Lenthe, E.J. Baerends, J.G. Snijders, Relativistic regular two-component Hamiltonians, J. Chem. Phys. 99 (1993) 4597–4610. https://doi.org/10.1063/1.466059.

[194] R. Baková, M. Chergui, C. Daniel, A. Vlček Jr., S. Záliš, Relativistic effects in spectroscopy and photophysics of heavy-metal complexes illustrated by spin–orbit calculations of [Re(imidazole)(CO)3(phen)]+, Coord. Chem. Rev. 255 (2011) 975–989. https://doi.org/10.1016/j.ccr.2010.12.027.

[195] S. Di Mo, W.Y. Ching, Electronic and optical properties of three phases of titanium dioxide: Rutile, anatase, and brookite, Phys. Rev. B. 51 (1995) 13023–13032. https://doi.org/10.1103/PhysRevB.51.13023.

[196] V.S. Stepanyuk, A.A. Grigorenko, A.A. Katsnelson, O. V. Farberovich, A. Szász, V. V. Mikhailin, Electronic structure and optical properties of MgS, Phys. Status Solidi. 174 (1992) 289–294. https://doi.org/10.1002/pssb.2221740129.

[197] Z.-X. Shen, R.S. List, D.S. Dessau, B.O. Wells, O. Jepsen, A.J. Arko, R. Barttlet, C.K. Shih, F. Parmigiani, J.C. Huang, P.A.P. Lindberg, Electronic structure of NiO: Correlation and band effects, Phys. Rev. B. 44 (1991) 3604–3626. https://doi.org/10.1103/PhysRevB.44.3604.

[198] Y.F. Zhang, W. Lin, Y. Li, K.N. Ding, J.Q. Li, A theoretical study on the electronic structures of TiO2: Effect of Hartree - Fock exchange, J. Phys. Chem. B. 109 (2005) 19270–19277. https://doi.org/10.1021/jp0523625.

[199] C.H. Patterson, Comparison of Hybrid Density Functional, Hartree–Fock, and GW Calculations on NiO, Int. J. Quantum Chem. 106 (2006) 3383–3386. https://doi.org/10.1002/qua.21136.

[200] F. Wang, C. Di Valentin, G. Pacchioni, Electronic and structural properties of WO3: A systematic hybrid DFT study, J. Phys. Chem. C. 115 (2011) 8345–8353. https://doi.org/10.1021/jp201057m.

[201] K.C. Ko, O. Lamiel-García, J.Y. Lee, F. Illas, Performance of a modified hybrid functional in the simultaneous description of stoichiometric and reduced TiO2 polymorphs, Phys. Chem. Chem. Phys. 18 (2016) 12357–12367. https://doi.org/10.1039/c6cp00912c.

[202] P. Broqvist, A. Alkauskas, A. Pasquarello, Hybrid-functional calculations with plane-wave basis sets: Effect of singularity correction on total energies, energy eigenvalues, and defect energy levels, Phys. Rev. B - Condens. Matter Mater. Phys. 80 (2009) 1–13. https://doi.org/10.1103/PhysRevB.80.085114.

[203] L.G. Ferreira, M. Marques, L.K. Teles, Approximation to density functional theory for the calculation of band gaps of semiconductors, Phys. Rev. B - Condens. Matter Mater. Phys. 78 (2008) 1–9. https://doi.org/10.1103/PhysRevB.78.125116.

[204] L. Reining, The GW approximation: content, successes and limitations, Wiley Interdiscip. Rev. Comput. Mol. Sci. 8 (2018) 1–26. https://doi.org/10.1002/wcms.1344.

[205] P. Umari, L. Giacomazzi, F. De Angelis, M. Pastore, S. Baroni, Energy-level alignment in organic dye-sensitized TiO2 from GW calculations, J. Chem. Phys. 139 (2013) 0–9. https://doi.org/10.1063/1.4809994.

[206] C. Verdi, E. Mosconi, F. De Angelis, M. Marsili, P. Umari, Alignment of energy levels in dye/semiconductor interfaces by GW calculations: Effects due to coadsorption of solvent molecules, Phys. Rev. B - Condens. Matter Mater. Phys. 90 (2014) 1–7. https://doi.org/10.1103/PhysRevB.90.155410.

[207] J.M.P. Martirez, E.A. Carter, Metal-to-Ligand Charge-Transfer Spectrum of a Ru-Bipyridine-Sensitized TiO2Cluster from Embedded Multiconfigurational Excited-

State Theory, J. Phys. Chem. A. 125 (2021) 4998–5013. https://doi.org/10.1021/acs.jpca.1c02628.

[208] X. Blase, I. Duchemin, D. Jacquemin, The Bethe-Salpeter equation in chemistry: Relations with TD-DFT, applications and challenges, Chem. Soc. Rev. 47 (2018) 1022–1043. https://doi.org/10.1039/c7cs00049a.

[209] X. Blase, I. Duchemin, D. Jacquemin, P.F. Loos, The Bethe-Salpeter Equation Formalism: From Physics to Chemistry, J. Phys. Chem. Lett. 11 (2020) 7371–7382. https://doi.org/10.1021/acs.jpclett.0c01875.

[210] M. Marsili, E. Mosconi, F. De Angelis, P. Umari, Large-scale GW -BSE calculations with N3 scaling: Excitonic effects in dye-sensitized solar cells, Phys. Rev. B. 95 (2017) 1–8. https://doi.org/10.1103/PhysRevB.95.075415.

[211] D. Escudero, I. Duchemin, X. Blase, D. Jacquemin, Modeling the Photochrome-TiO2 Interface with Bethe-Salpeter and Time-Dependent Density Functional Theory Methods, J. Phys. Chem. Lett. 8 (2017) 936–940. https://doi.org/10.1021/acs.jpclett.7b00015.

[212] M. Elstner, D. Porezag, G. Jungnickel, M.H. J. Elsner, T. Frauenheim, S. Suhai, G. Seifert, Self-consistent-charge density-functional tight-binding method for simulations of complex materials properties, Phys. Rev. B. 58 (1998) 7260. https://doi.org/10.1007/0-387-24006-3_3.

[213] G. Dolgonos, B. Aradi, N.H. Moreira, T. Frauenheim, An improved self-consistent-charge density-functional tight-binding (SCC-DFTB) set of parameters for simulation of bulk and molecular systems involving titanium, J. Chem. Theory Comput. 6 (2010) 266–278. https://doi.org/10.1021/ct900422c.

[214] W.J. Fan, Y.Z. Chang, J.L. Zhao, Z.N. Xu, D.Z. Tan, Y.G. Chen, A theoretical study of fused thiophene modified anthracene-based organic dyes for dye-sensitized solar cell applications, New J. Chem. 42 (2018) 20163–20170. https://doi.org/10.1039/c8nj03592j.

[215] L.L. Estrella, M.P. Balanay, D.H. Kim, The Effect of Donor Group Rigidification on the Electronic and Optical Properties of Arylamine-Based Metal-Free Dyes for Dye-Sensitized Solar Cells: A Computational Study, 2016. https://doi.org/10.1021/acs.jpca.6b03271.

[216] W. Zhang, P. Heng, H. Su, T. Ren, L. Wang, J. Zhang, Rational Design of High-Efficiency Organic Dyes in Dye-Sensitized Solar Cells by Multiscale Simulations, J. Phys. Chem. C. 122 (2018) 25219–25228. https://doi.org/10.1021/acs.jpcc.8b08750.

[217] S. Feng, Q.S. Li, P.P. Sun, T.A. Niehaus, Z.S. Li, Dynamic Characteristics of Aggregation Effects of Organic Dyes in Dye-Sensitized Solar Cells, ACS Appl. Mater. Interfaces. 7 (2015) 22504–22514. https://doi.org/10.1021/acsami.5b06743.

[218] J. Yang, X.L. Peng, Z.Z. Sun, S. Feng, W.L. Ding, H.Y. He, Z.S. Li, Understanding the effects of the co-sensitizing ratio on the surface potential, electron injection efficiency, and Förster resonance energy transfer, Phys. Chem. Chem. Phys. 22 (2020) 5568–5576. https://doi.org/10.1039/c9cp06028f.

[219] J.P. Menzel, A. Papadopoulos, J. Belić, H.J.M. de Groot, L. Visscher, F. Buda, Photoinduced electron injection in a fully solvated dye-sensitized photoanode: A dynamical semiempirical study, J. Phys. Chem. C. 124 (2020) 27965–27976. https://doi.org/10.1021/acs.jpcc.0c09551.

[220] S. Mukherjee, C. Liu, E. Jakubikova, Comparison of interfacial electron transfer efficiency in [Fe(ctpy)2]2+-TiO2 and [Fe(cCNC)2]2+-TiO2 Assemblies: Importance of conformational sampling, J. Phys. Chem. A. 122 (2018) 1821–1830. https://doi.org/10.1021/acs.jpca.7b10932.

[221] D.M. Marquez, C.G. Sánchez, Quantum efficiency of the photo-induced electronic transfer in dye-TiO2 complexes, Phys. Chem. Chem. Phys. 20 (2018) 26280–26287. https://doi.org/10.1039/c8cp04625e.

[222] J.P. Muscat, D.M. Newns, Chemisorption on Metals, Prog. Surf. Sci. 9 (1978) 1–43. https://doi.org/10.1016/0079-6816(78)90005-9.

[223] P. Persson, M.J. Lundqvist, R. Ernstorfer, W.A. Goddard, F. Willig, Quantum chemical calculations of the influence of anchor-cum-spacer groups on femtosecond electron transfer times in dye-sensitized semiconductor nanocrystals, J. Chem. Theory Comput. 2 (2006) 441–451. https://doi.org/10.1021/ct050141x.

[224] I. Kondov, M. Cížek, C. Benesch, H. Wang, M. Thoss, Quantum dynamics of photoinduced electron-transfer reactions in dye-semiconductor systems: First-principles description and application to coumarin 343-TiO2, J. Phys. Chem. C. 111 (2007) 11970–11981. https://doi.org/10.1021/jp072217m.

[225] J.C. Tremblay, T. Klamroth, P. Saalfrank, Time-dependent configuration-interaction calculations of laser-driven dynamics in presence of dissipation, J. Chem. Phys. 129 (2008) 0–8. https://doi.org/10.1063/1.2972126.

[226] G. Hermann, J.C. Tremblay, Ultrafast photoelectron migration in dye-sensitized solar cells: Influence of the binding mode and many-body interactions, J. Chem. Phys. 145 (2016). https://doi.org/10.1063/1.4966260.

[227] D. Sulzer, K. Yasuda, Resonance State Method for Electron Injection in Dye Sensitized Solar Cells, J. Chem. Theory Comput. 14 (2018) 5090–5104. https://doi.org/10.1021/acs.jctc.8b00364.

[228] D. Sulzer, S. Iuchi, K. Yasuda, A new method to evaluate excited states lifetimes based on green's function: Application to dye-sensitized solar cells, J. Chem. Theory Comput. 12 (2016) 3074–3086. https://doi.org/10.1021/acs.jctc.6b00181.

[229] W.R. Duncan, O. V. Prezhdo, Theoretical studies of photoinduced electron transfer in dye-sensitized TiO2, Annu. Rev. Phys. Chem. 58 (2007) 143–184. https://doi.org/10.1146/annurev.physchem.58.052306.144054.

[230] A. V. Akimov, A.J. Neukirch, O. V. Prezhdo, Theoretical insights into photoinduced charge transfer and catalysis at oxide interfaces, Chem. Rev. 113 (2013) 4496–4565. https://doi.org/10.1021/cr3004899.

[231] C.R. Tichnell, J.N. Miller, C. Liu, S. Mukherjee, E. Jakubikova, J.K. Mccusker, Influence of Electrolyte Composition on Ultrafast Interfacial Electron Transfer in Fe-Sensitized TiO2-Based Solar Cells, J. Phys. Chem. C. 124 (2020) 1794–1811. https://doi.org/10.1021/acs.jpcc.9b09404.

[232] L.G.C. Rego, V.S. Batista, Quantum dynamics simulations of interfacial electron transfer in sensitized TiO2 semiconductors, J. Am. Chem. Soc. 125 (2003) 7989–7997. https://doi.org/10.1021/ja0346330.

[233] E. Jakubikova, R.C. Snoeberger, V.S. Batista, R.L. Martin, E.R. Batista, Interfacial electron transfer in TiO2 surfaces sensitized with Ru(II)-polypyridine complexes, J. Phys. Chem. A. 113 (2009) 12532–12540. https://doi.org/10.1021/jp903966n.

[234] W. Stier, O. V. Prezhdo, Non-adiabatic molecular dynamics simulation of ultrafast

solar cell electron transfer, J. Mol. Struct. THEOCHEM. 630 (2003) 33–43. https://doi.org/10.1016/S0166-1280(03)00167-2.

[235] W.R. Duncan, W.M. Stier, Ab Initio Nonadiabatic Molecular Dynamics of the Ultrafast Electron Injection across the Alizarin−TiO2 Interface - Journal of the American Chemical Society (ACS Publications), J. Am. …. (2005) 7941–7951. http://pubs.acs.org/doi/abs/10.1021/ja042156v%0Apapers3://publication/uuid/D2F39C62-62C2-4192-AEB7-6FB4A4ECDBDA.

[236] J. Li, H. Wang, P. Persson, M. Thoss, Photoinduced electron transfer processes in dye-semiconductor systems with different spacer groups, J. Chem. Phys. 137 (2012). https://doi.org/10.1063/1.4746768.

[237] W. Stier, O. V. Prezhdo, Nonadiabatic Molecular Dynamics Simulation of Light-Induced Electron Transfer from an Anchored Molecular Electron Donor to a Semiconductor Acceptor, J. Phys. Chem. B. 106 (2002) 8047–8054. https://doi.org/10.1021/jp014267b.

[238] A. Monti, C.F.A. Negre, V.S. Batista, L.G.C. Rego, H.J.M. De Groot, F. Buda, Crucial role of nuclear dynamics for electron injection in a dye-semiconductor complex, J. Phys. Chem. Lett. 6 (2015) 2393–2398. https://doi.org/10.1021/acs.jpclett.5b00876.

[239] S. Meng, E. Kaxiras, Electron and hole dynamics in dye-sensitized solar cells: Influencing factors and systematic trends, Nano Lett. 10 (2010) 1238–1247. https://doi.org/10.1021/nl100442e.

[240] W. Ma, Y. Jiao, S. Meng, Predicting energy conversion efficiency of dye solar cells from first principles, J. Phys. Chem. C. 118 (2014) 16447–16457.

https://doi.org/10.1021/jp410982e.

[241] Y. Wen, L. Fu, G. Li, J. Ma, H. Ma, Accelerated Discovery of Potential Organic Dyes for Dye-Sensitized Solar Cells by Interpretable Machine Learning Models and Virtual Screening, Sol. RRL. 4 (2020) 1–11. https://doi.org/10.1002/solr.202000110.

[242] G.R. Kandregula, D.K. Murugaiah, N.A. Murugan, Data-driven Approach Towards Identifying Dye-Sensitizer Molecules for Higher Power Conversion Efficiency in Solar Cells, New J. Chem. (2022). https://doi.org/10.1039/D1NJ05498H.

[243] C.B. Cooper, E.J. Beard, Á. Vázquez-Mayagoitia, L. Stan, G.B.G. Stenning, D.W. Nye, J.A. Vigil, T. Tomar, J. Jia, G.B. Bodedla, S. Chen, L. Gallego, S. Franco, A. Carella, K.R.J. Thomas, S. Xue, X. Zhu, J.M. Cole, Design-to-Device Approach Affords Panchromatic Co-Sensitized Solar Cells, Adv. Energy Mater. 9 (2019) 1–10. https://doi.org/10.1002/aenm.201802820.

[244] S.S. Sutar, S.M. Patil, S.J. Kadam, R.K. Kamat, D.K. Kim, T.D. Dongale, Analysis and Prediction of Hydrothermally Synthesized ZnO-Based Dye-Sensitized Solar Cell Properties Using Statistical and Machine-Learning Techniques, ACS Omega. 6 (2021) 29982–29992. https://doi.org/10.1021/acsomega.1c04521.

[245] V. Venkatraman, A.E. Yemene, J. de Mello, Prediction of Absorption Spectrum Shifts in Dyes Adsorbed on Titania, Sci. Rep. 9 (2019) 1–13. https://doi.org/10.1038/s41598-019-53534-2.

[246] H. Rensmo, S. Södergren, L. Patthey, K. Westermark, L. Vayssieres, O. Kohle, P.A. Brühwiler, A. Hagfeldt, H. Siegbahn, The electronic structure of the cis-

bis(4,4′-dicarboxy-2,2′-bipyridine)-bis(isothiocyanato)ruthenium(II) complex and its ligand 2,2′-bipyridyl-4,4′-dicarboxylic acid studied with electron spectroscopy, Chem. Phys. Lett. 274 (1997) 51–57. https://doi.org/10.1016/S0009-2614(97)00670-2.

[247] S. Fantacci, F. De Angelis, A. Selloni, Absorption Spectrum and Solvatochromism of the [Ru(4,4′-COOH-2,2′ bpy)2(NCS)2] Molecular Dye by Time Dependent Density Functional Theory, J. Am. Chem. Soc. 125 (2003) 4381–4387. https://doi.org/10.1021/ja0207910.

[248] J.E. Monat, J.H. Rodriguez, J.K. McCusker, Ground- and excited-state electronic structures of the solar cell sensitizer bis(4,4′-dicarboxylato-2,2′-bipyridine)bis(isothiocyanato)ruthenium(II), J. Phys. Chem. A. 106 (2002) 7399–7406. https://doi.org/10.1021/jp020927g.

[249] F. De Angelis, S. Fantacci, A. Selloni, M.K. Nazeeruddin, Time dependent density functional theory study of the absorption spectrum of the [Ru(4,4′-COO--2,2′-bpy)2(X) 2]4- (X = NCS, Cl) dyes in water solution, Chem. Phys. Lett. 415 (2005) 115–120. https://doi.org/10.1016/j.cplett.2005.08.044.

[250] A. Chantzis, T. Very, A. Monari, X. Assfeld, Improved treatment of surrounding effects: UV/vis absorption properties of a solvated Ru(II) complex, J. Chem. Theory Comput. 8 (2012) 1536–1541. https://doi.org/10.1021/ct300129c.

[251] M.F. Charlot, A. Aukauloo, Highlighting the role of the medium in DFT analysis of the photophysical properties of ruthenium(II) polypyridine-type complexes, J. Phys. Chem. A. 111 (2007) 11661–11672. https://doi.org/10.1021/jp074605u.

[252] S.R. Stoyanov, J.M. Villegas, D. Paul Rillema, The charge transfer band solvent-

dependence of [Ru(bpy)2(CN x)Cl]+, CNx=2,6-dimethylphenylisocyanide: A polarizable continuum model/time-dependent density functional theory study, Inorg. Chem. Commun. 7 (2004) 838–841. https://doi.org/10.1016/j.inoche.2004.05.003.

[253] S. Fantacci, F. De Angelis, A. Sgamellotti, N. Re, A TDDFT study of the ruthenium(II) polyazaaromatic complex [Ru(dppz)(phen) 2] 2+ in solution, Chem. Phys. Lett. 396 (2004) 43–48. https://doi.org/10.1016/j.cplett.2004.07.101.

[254] M.K. Nazeeruddin, F. De Angelis, S. Fantacci, A. Selloni, G. Viscardi, P. Liska, S. Ito, B. Takeru, M. Grätzel, Combined Experimental and DFT-TDDFT Computational Study of Photoelectrochemical Cell Ruthenium Sensitizers, J. Am. Chem. Soc. 127 (2005) 16835–16847. https://doi.org/10.1021/ja052467l.

[255] M.K. Nazeeruddin, P. Péchy, M. Grätzel, Efficient panchromatic sensitization of nanocrystalline TiO2 films by a black dye based on a trithiocyanato-ruthenium complex, Chem. Commun. 1 (1997) 1705–1706. https://doi.org/10.1039/a703277c.

[256] T. Kinoshita, J.T. Dy, S. Uchida, T. Kubo, H. Segawa, Wideband dye-sensitized solar cells employing a phosphine-coordinated ruthenium sensitizer, Nat. Photonics. 7 (2013) 535–539. https://doi.org/10.1038/nphoton.2013.136.

[257] T. Kinoshita, K. Nonomura, N.J. Jeon, F. Giordano, A. Abate, S. Uchida, T. Kubo, S. Il Seok, M.K. Nazeeruddin, A. Hagfeldt, M. Grätzel, H. Segawa, Spectral splitting photovoltaics using perovskite and wideband dye-sensitized solar cells, Nat. Commun. 6 (2015) 1–8. https://doi.org/10.1038/ncomms9834.

[258] T. Kinoshita, M. Otsubo, T. Ono, H. Segawa, Enhancement of Near-Infrared Singlet-Triplet Absorption of Ru(II) Sensitizers for Improving Conversion

Efficiency of Solar Cells, ACS Appl. Energy Mater. 4 (2021) 7052–7063. https://doi.org/10.1021/acsaem.1c01113.

[259] S. Fantacci, F. De Angelis, Ab Initio Modeling of Solar Cell Dye Sensitizers: The Hunt for Red Photons Continues, Eur. J. Inorg. Chem. 2019 (2019) 743–750. https://doi.org/10.1002/ejic.201801258.

[260] C. Daul, E.J. Baerends, P. Vernooijs, A Density Functional Study of the MLCT States of [Ru(bpy)3]2+ in D3 Symmetry, Inorg. Chem. 33 (1994) 3538–3543. https://doi.org/10.1021/ic00094a017.

[261] E.M.J. Johansson, M. Odelius, S. Plogmaker, M. Gorgoi, S. Svensson, H. Siegbahn, H. Rensmo, Spin-orbit coupling and metala-ligand interactions in Fe(II), Ru(II), and Os(II) complexes, J. Phys. Chem. C. 114 (2010) 10314–10322. https://doi.org/10.1021/jp103884c.

[262] E. Ronca, F. De Angelis, S. Fantacci, Time-dependent density functional theory modeling of spin-orbit coupling in ruthenium and osmium solar cell sensitizers, J. Phys. Chem. C. 118 (2014) 17067–17078. https://doi.org/10.1021/jp500869r.

[263] L. Han, A. Islam, H. Chen, C. Malapaka, B. Chiranjeevi, S. Zhang, X. Yang, M. Yanagida, High-efficiency dye-sensitized solar cell with a novel co-adsorbent, Energy Environ. Sci. 5 (2012) 6057–6060. https://doi.org/10.1039/c2ee03418b.

[264] S. Fantacci, E. Ronca, F. De Angelis, Impact of spin-orbit coupling on photocurrent generation in ruthenium dye-sensitized solar cells, J. Phys. Chem. Lett. 5 (2014) 375–380. https://doi.org/10.1021/jz402544r.

[265] S. Kanno, Y. Imamura, M. Hada, Design of spin-forbidden transitions for polypyridyl metal complexes by time-dependent density functional theory

including spin-orbit interaction, Phys. Chem. Chem. Phys. 18 (2016) 14466–14478. https://doi.org/10.1039/c6cp01461e.

[266] Y. Imamura, M. Kamiya, T. Nakajima, Two-component relativistic time-dependent density functional theory study on spin-forbidden transitions for metal polypyridyl complexes, Chem. Phys. Lett. 635 (2015) 152–156. https://doi.org/10.1016/j.cplett.2015.06.057.

[267] Y. Imamura, M. Kamiya, T. Nakajima, Theoretical study on spin-forbidden transitions of osmium complexes by two-component relativistic time-dependent density functional theory, Chem. Phys. Lett. 648 (2016) 60–65. https://doi.org/10.1016/j.cplett.2016.01.018.

[268] G. Auböck, M. Chergui, Sub-50-fs photoinduced spin crossover in [Fe(bpy)3]2+, Nat. Chem. 7 (2015) 629–633. https://doi.org/10.1038/nchem.2305.

[269] C. Consani, M. Prémont-Schwarz, A. Elnahhas, C. Bressler, F. Van Mourik, A. Cannizzo, M. Chergui, Vibrational coherences and relaxation in the high-spin state of aqueous [FeIIbpy3]2, Angew. Chemie - Int. Ed. 48 (2009) 7184–7187. https://doi.org/10.1002/anie.200902728.

[270] D.C. Ashley, E. Jakubikova, Ironing out the photochemical and spin-crossover behavior of Fe(II) coordination compounds with computational chemistry, Coord. Chem. Rev. 337 (2017) 97–111. https://doi.org/10.1016/j.ccr.2017.02.005.

[271] J. Nance, D.N. Bowman, S. Mukherjee, C.T. Kelley, E. Jakubikova, Insights into the Spin-State Transitions in [Fe(tpy)2]2+: Importance of the Terpyridine Rocking Motion, Inorg. Chem. 54 (2015) 11259–11268. https://doi.org/10.1021/acs.inorgchem.5b01747.

[272] I.M. Dixon, F. Alary, M. Boggio-Pasqua, J. Heully, Reversing the relative 3MLCT–3MC order in Fe(II) complexes using cyclometallating ligands: a computational study aiming at luminescent Fe(II) complexes, Dalt. Trans. 44 (2015) 13498–13503. https://doi.org/10.1039/c5dt01214g.

[273] P. Chábera, Y. Liu, O. Prakash, E. Thyrhaug, A. El Nahhas, A. Honarfar, S. Essén, L.A. Fredin, T.C.B. Harlang, K.S. Kjær, K. Handrup, F. Ericson, H. Tatsuno, K. Morgan, J. Schnadt, L. Häggström, T. Ericsson, A. Sobkowiak, S. Lidin, P. Huang, S. Styring, J. Uhlig, J. Bendix, R. Lomoth, V. Sundström, P. Persson, K. Wärnmark, A low-spin Fe(III) complex with 100-ps ligand-to-metal charge transfer photoluminescence, Nature. 543 (2017) 695–699. https://doi.org/10.1038/nature21430.

[274] Y. Liu, K.S. Kjær, L.A. Fredin, P. Chábera, T. Harlang, S.E. Canton, S. Lidin, J. Zhang, R. Lomoth, K.E. Bergquist, P. Persson, K. Wärnmark, V. Sundström, A heteroleptic ferrous complex with mesoionic bis(1,2,3-triazol-5-ylidene) ligands: Taming the MLCT excited state of iron(II), Chem. - A Eur. J. 21 (2015) 3628–3639. https://doi.org/10.1002/chem.201405184.

[275] S.G. Shepard, S.M. Fatur, A.K. Rappé, N.H. Damrauer, Highly Strained Iron(II) Polypyridines: Exploiting the Quintet Manifold to Extend the Lifetime of MLCT Excited States, J. Am. Chem. Soc. 138 (2016) 2949–2952. https://doi.org/10.1021/jacs.5b13524.

[276] S.M. Fatur, S.G. Shepard, R.F. Higgins, M.P. Shores, N.H. Damrauer, A Synthetically Tunable System to Control MLCT Excited-State Lifetimes and Spin States in Iron(II) Polypyridines, J. Am. Chem. Soc. 139 (2017) 4493–4505.

https://doi.org/10.1021/jacs.7b00700.

[277] A. Francés-Monerris, P.C. Gros, X. Assfeld, A. Monari, M. Pastore, Toward Luminescent Iron Complexes: Unravelling the Photophysics by Computing Potential Energy Surfaces, ChemPhotoChem. 3 (2019) 666–683. https://doi.org/10.1002/cptc.201900100.

[278] W. Zhang, K.S. Kjær, R. Alonso-Mori, U. Bergmann, M. Chollet, L.A. Fredin, R.G. Hadt, R.W. Hartsock, T. Harlang, T. Kroll, K. Kubiček, H.T. Lemke, H.W. Liang, Y. Liu, M.M. Nielsen, P. Persson, J.S. Robinson, E.I. Solomon, Z. Sun, D. Sokaras, T.B. Van Driel, T.C. Weng, D. Zhu, K. Wärnmark, V. Sundström, K.J. Gaffney, Manipulating charge transfer excited state relaxation and spin crossover in iron coordination complexes with ligand substitution, Chem. Sci. 8 (2016) 515–523. https://doi.org/10.1039/C6SC03070J.

[279] L.A. Fredin, K. Wärnmark, V. Sundström, P. Persson, Molecular and Interfacial Calculations of Iron(II) Light Harvesters, ChemSusChem. 9 (2016) 667–675. https://doi.org/10.1002/cssc.201600062.

[280] P. Chábera, K.S. Kjaer, O. Prakash, A. Honarfar, Y. Liu, L.A. Fredin, T.C.B. Harlang, S. Lidin, J. Uhlig, V. Sundström, R. Lomoth, P. Persson, K. Wärnmark, FeII Hexa N-Heterocyclic Carbene Complex with a 528 ps Metal-To-Ligand Charge-Transfer Excited-State Lifetime, J. Phys. Chem. Lett. 9 (2018) 459–463. https://doi.org/10.1021/acs.jpclett.7b02962.

[281] C. Sousa, C. De Graaf, A. Rudavskyi, R. Broer, J. Tatchen, M. Etinski, C.M. Marian, Ultrafast deactivation mechanism of the excited singlet in the light-induced spin crossover of [Fe(2,2-bipyridine)3]2+, Chem. - A Eur. J. 19 (2013)

17541–17551. https://doi.org/10.1002/chem.201302992.

[282] A. Hauser, C. Enachescu, M.L. Daku, A. Vargas, N. Amstutz, Low-temperature lifetimes of metastable high-spin states in spin-crossover and in low-spin iron(II) compounds: The rule and exceptions to the rule, Coord. Chem. Rev. 250 (2006) 1642–1652. https://doi.org/10.1016/j.ccr.2005.12.006.

[283] M. Pápai, G. Vanko, C. De Graaf, T. Rozgonyi, Theoretical Investigation of the Electronic Structure of Fe(II) Complexes at Spin-State Transitions, J. Chem. Theory Comput. 9 (2013) 509−519. https://doi.org/10.1021/ct300932n.

[284] I.M. Dixon, F. Alary, M. Boggio-Pasqua, J.L. Heully, The (N4C2)2- donor set as promising motif for bis(tridentate) iron(II) photoactive compounds, Inorg. Chem. 52 (2013) 13369–13374. https://doi.org/10.1021/ic402453p.

[285] K. Magra, E. Domenichini, A. Francés-Monerris, C. Cebrián, M. Beley, M. Darari, M. Pastore, A. Monari, X. Assfeld, S. Haacke, P.C. Gros, Impact of the fac/ mer Isomerism on the Excited-State Dynamics of Pyridyl-carbene Fe(II) Complexes, Inorg. Chem. 58 (2019) 5069–5081. https://doi.org/10.1021/acs.inorgchem.9b00138.

[286] A. Francés-Monerris, K. Magra, M. Darari, C. Cebrián, M. Beley, E. Domenichini, S. Haacke, M. Pastore, X. Assfeld, P.C. Gros, A. Monari, Synthesis and Computational Study of a Pyridylcarbene Fe(II) Complex: Unexpected Effects of fac/ mer Isomerism in Metal-to-Ligand Triplet Potential Energy Surfaces, Inorg. Chem. 57 (2018) 10431–10441. https://doi.org/10.1021/acs.inorgchem.8b01695.

[287] G. Henkelman, B.P. Uberuaga, H. Jónsson, Climbing image nudged elastic band method for finding saddle points and minimum energy paths, J. Chem. Phys. 113

(2000) 9901–9904. https://doi.org/10.1063/1.1329672.

[288] H. Köuppel, W. Domcke, L.S. Cederbaum, Multimode Molecular Dynamics Beyond the Born-Oppenheimer Approximation, Adv. Chem. Phys. 57 (1984) 59–246. https://doi.org/10.1002/9780470142813.ch2.

[289] M. Pápai, M. Simmermacher, T.J. Penfold, K.B. Møller, T. Rozgonyi, How to Excite Nuclear Wavepackets into Electronically Degenerate States in Spin-Vibronic Quantum Dynamics Simulations, J. Chem. Theory Comput. 14 (2018) 3967–3974. https://doi.org/10.1021/acs.jctc.8b00135.

[290] F. Plasser, S. Gómez, M.F.S.J. Menger, S. Mai, L. González, Highly efficient surface hopping dynamics using a linear vibronic coupling model, Phys. Chem. Chem. Phys. 21 (2019) 57–69. https://doi.org/10.1039/c8cp05662e.

[291] J.P. Zobel, O.S. Bokareva, P. Zimmer, C. Wölper, M. Bauer, L. González, Intersystem Crossing and Triplet Dynamics in an Iron(II) N-Heterocyclic Carbene Photosensitizer, Inorg. Chem. 59 (2020) 14666–14678. https://doi.org/10.1021/acs.inorgchem.0c02147.

[292] M. Pastore, T. Duchanois, L. Liu, A. Monari, X. Assfeld, S. Haacke, P.C. Gros, Interfacial charge separation and photovoltaic efficiency in Fe(II)-carbene sensitized solar cells, Phys. Chem. Chem. Phys. 18 (2016) 28069–28081. https://doi.org/10.1039/c6cp05535d.

[293] M. Becker, V. Wyss, C.E. Housecroft, E.C. Constable, The influence of alkyl chains on the performance of DSCs employing iron(ii) N-heterocyclic carbene sensitizers, Dalt. Trans. 50 (2021) 16961–16969. https://doi.org/10.1039/d1dt03252f.

[294] M. Becker, C.E. Housecroft, E.C. Constable, Electrolyte tuning in iron(II)-based dye-sensitized solar cells: Different ionic liquids and I2 concentrations, Materials (Basel). 14 (2021). https://doi.org/10.3390/ma14113053.

[295] M. Karpacheva, C.E. Housecroft, E.C. Constable, Electrolyte tuning in dye-sensitized solar cells with N-heterocyclic carbene (NHC) iron(II) sensitizers, Beilstein J. Nanotechnol. 9 (2018) 3069–3078. https://doi.org/10.3762/bjnano.9.285.

[296] P. Persson, M.J. Lundqvist, Calculated structural and electronic interactions of the ruthenium dye N3 with a titanium dioxide nanocrystal, J. Phys. Chem. B. 109 (2005) 11918–11924. https://doi.org/10.1021/jp050513y.

[297] N. Martsinovich, F. Ambrosio, A. Troisi, Adsorption and electron injection of the N3 metal-organic dye on the TiO2 rutile (110) surface, Phys. Chem. Chem. Phys. 14 (2012) 16668–16676. https://doi.org/10.1039/c2cp42350b.

[298] F. Labat, I. Ciofini, C. Adamo, Revisiting the importance of dye binding mode in dye-sensitized solar cells: A periodic viewpoint, J. Mater. Chem. 22 (2012) 12205–12211. https://doi.org/10.1039/c2jm31119d.

[299] S. Fantacci, M.G. Lobello, F. De Angelis, Everything you always wanted to know about black dye (but were afraid to ask): A DFT/TDDFT investigation, Chimia (Aarau). 67 (2013) 121–128. https://doi.org/10.2533/chimia.2013.121.

[300] K. Sodeyama, M. Sumita, C. ORourke, U. Terranova, A. Islam, L. Han, D.R. Bowler, Y. Tateyama, Protonated carboxyl anchor for stable adsorption of Ru N749 dye (black dye) on a TiO 2 anatase (101) surface, J. Phys. Chem. Lett. 3 (2012) 472–477. https://doi.org/10.1021/jz201583n.

[301] S.H. Liu, H. Fu, Y.M. Cheng, K.L. Wu, S. Te Ho, Y. Chi, P.T. Chou, Theoretical study of N749 dyes anchoring on the (TiO 2) 28 surface in DSSCs and their electronic absorption Properties, J. Phys. Chem. C. 116 (2012) 16338–16345. https://doi.org/10.1021/jp3006074.

[302] S. Mukherjee, D.N. Bowman, E. Jakubikova, Cyclometalated Fe(II) complexes as sensitizers in dye-sensitized solar cells, Inorg. Chem. 54 (2015) 560–569. https://doi.org/10.1021/ic502438g.

[303] E. Galoppini, Strike while the iron is cold, Nat. Chem. 7 (2015) 861–862. https://doi.org/10.1038/nchem.2373.

[304] S. Agrawal, T. Leijtens, E. Ronca, M. Pastore, H. Snaith, F. De Angelis, Modeling the effect of ionic additives on the optical and electronic properties of a dye-sensitized TiO2 heterointerface: Absorption, charge injection and aggregation, J. Mater. Chem. A. 1 (2013) 14675–14685. https://doi.org/10.1039/c3ta12917a.